

promoting access to White Rose research papers



Universities of Leeds, Sheffield and York
<http://eprints.whiterose.ac.uk/>

This is the author's version of an article published in **Energy and Environmental Science**

White Rose Research Online URL for this paper:

<http://eprints.whiterose.ac.uk/id/eprint/76058>

Published article:

Molinder, R, Comyn, TP, Hondow, N, Parker, JE and Dupont, V (2012) *In situ X-ray diffraction of CaO based CO₂ sorbents*. Energy and Environmental Science, 5 (10). 8958 - 8969. ISSN 1754-5692

<http://dx.doi.org/10.1039/c2ee21779a>



In-situ X-ray diffraction of CaO based CO₂ sorbents

R. Molinder¹, T.P. Comyn^{2*}, N. Hondow², J.E. Parker³, V. Dupont¹

¹ *Energy Research Institute, ² Institute of Materials Research, School of Process, Environmental and Materials Engineering, The University of Leeds, LS2 9JT, UK,*

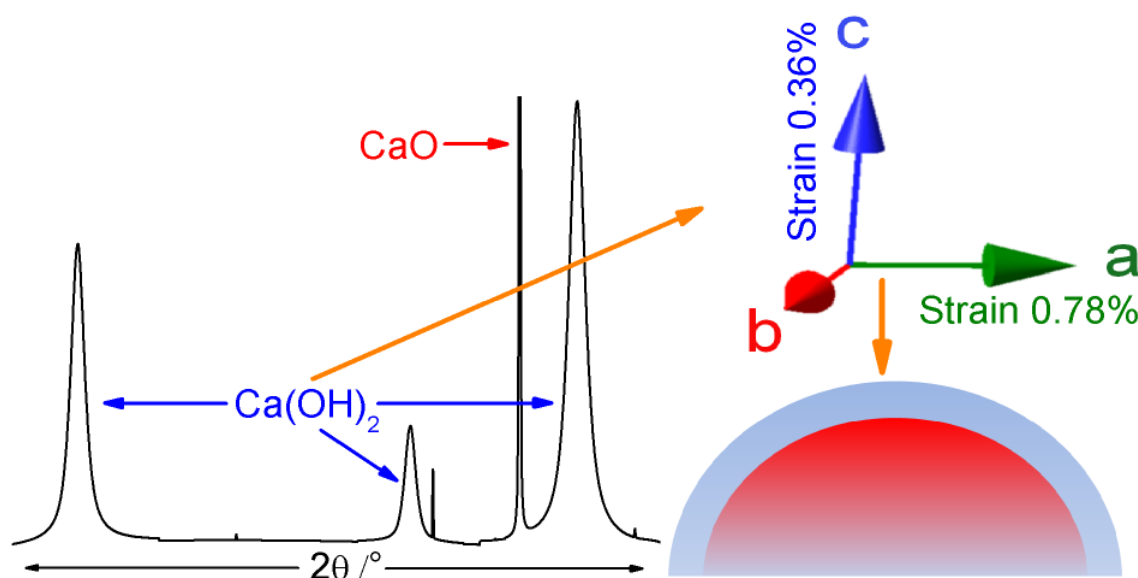
³ *Diamond Light Source Ltd, Diamond House, Harwell Science and Innovation Campus, Didcot, OX11 0DE, UK*

Abstract

In situ X-ray diffraction coupled with Rietveld refinement has been used to study CO₂ capture by CaO, Ca(OH)₂ and partially hydrated CaO, as a function of temperature. Phase quantification by Rietveld refinement was performed to monitor the conversion to CaCO₃ and the results were compared to those derived using thermogravimetric analysis (TGA). It was found that Ca(OH)₂ converted directly to 100% CaCO₃ without the formation of a CaO intermediate, at ca. 600 °C. Both pure CaO and partially hydrated CaO (33.6 wt% Ca(OH)₂) reached the same capture capacity, containing approximately 65 wt% CaCO₃ at 800 °C. It was possible to provide direct evidence of the capture mechanism. The stresses in the Ca(OH)₂ phase of the partially hydrated CaO were found to be more than 20 times higher than its strength, leading to disintegration and the generation of nano-sized crystallites. The crystallite size determined using diffraction (75×16 nm) was in good agreement with the average crystallite size observed using TEM (of 83×16 nm). Electron diffraction images confirmed coexistence of CaO and Ca(OH)₂. The analysis provides an explanation of the enhanced capture /disintegration observed in CaO in the presence of steam.

Keywords: Rietveld analysis, *in-situ* X-ray diffraction, CaO, CO₂ capture, hydration, capture mechanism, attrition, regeneration, synchrotron.

Graphical abstract



In situ XRD, in conjunction with phase quantification using Rietveld analysis, was used successfully to study CO_2 capture in CaO and Ca(OH)_2 as well as in partially hydrated CaO . The work shows how *in situ* XRD can be used as a supplemental technique to TGA, by which the mechanism of capture and hydration can be elucidated.

1 Introduction

Concerns about global warming have prompted both national and international efforts to curb CO_2 emissions. CaO based materials are being considered as CO_2 sorbents for removal of CO_2 from flue gases at temperatures between $400\text{ }^\circ\text{C}$ and $800\text{ }^\circ\text{C}$. Applications include pre- and post-combustion carbon capture technologies.¹⁻¹⁰ In addition, with the growing replacement of fossil fuels by biomass sources, and due to the high oxygen content of biomass, many of the processes of thermochemical fuel upgrading generate significant CO_2 at medium-high temperatures.¹¹⁻¹² This provides the opportunity for *in situ* CO_2 capture in the $400\text{-}800\text{ }^\circ\text{C}$ range and for improved heat transfer arising from the coupling of the endothermic gasification reactions with the exothermicity of the CO_2 chemisorption. This results in lower reaction temperatures and lower fuel consumption.¹³⁻¹⁴ The advantages of CaO based materials as CO_2 sorbents for pre- and post-combustion CO_2 capture are their low cost, high abundance, large sorption capacity and fast reaction kinetics.¹⁵⁻¹⁷ However, a major shortcoming of CaO based materials as CO_2 sorbents is the degradation in sorption capacity after multiple capture and regeneration cycles, due to loss of surface area through sintering.¹⁸⁻
²¹ For large scale CO_2 capture, the cost of the CaO based material and the rate of surface area

loss are the parameters that exhibit the highest sensitivities towards the total cost.²² Hence, there is an economic incentive to maintain a high surface area of the sorbent over multiple CO₂ capture cycles.

Hydration has been shown to influence the properties of CaO based materials. Hydration during CO₂ capture can for example increase capture capacity. This has been achieved by the addition of steam.^{13,23,24} Hydration of calcined material followed by decomposition can be used as a regeneration method of sintered materials since it can restore a high surface area.²⁵⁻²⁸ A major drawback of hydration as a regeneration method is the reduced mechanical strength of the regenerated material.^{26,29,30} However, by hydrating in a CO₂ atmosphere, the reduction in mechanical strength can be retarded.³¹

Currently, thermogravimetric analysis (TGA) and bench scale reactors are the most common techniques for studying CO₂ capture by CaO based materials. TGA relies on monitoring the sample mass over time which can be used to measure formation of CaCO₃ and Ca(OH)₂ from CaO and vice versa. However, when formation and/or decomposition of CaCO₃ and Ca(OH)₂ occur simultaneously (*e.g.* during CO₂ capture in the presence of steam or during surface area regeneration by hydration), TGA cannot readily distinguish between a change in mass derived from CaCO₃ or Ca(OH)₂. It is possible to quantify outlet concentrations of gaseous products including CO₂ and H₂O by coupling TGA with mass spectrometry (MS). By doing so, Blamey *et al.*³² were able to simultaneously monitor mass change and steam evolution when studying a range of different Ca(OH)₂ sorbents. However, accurate quantification of outlet gases is made difficult by the small amounts of sample which the TGA apparatus will allow. Bench scale reactors can be sized to allow for larger sample mass so that reactor outlet gas concentrations and steam partial pressures can be accurately quantified.^{19,24,31,33} With this technique, outlet gas concentrations and steam partial pressure measurements are related to known inlet concentrations and partial pressures, allowing for rates of production or consumption to be calculated. To obtain extents of CO₂/H₂O intakes or releases, the rates require integrating over the reaction time, a calculation prone to error propagation and over-reliant on accurate knowledge of the duration of the reactions. This limits the ability to relate the measurements to accurate extent of formation and/or decomposition of CaCO₃ and Ca(OH)₂. Moreover, the larger sample mass used in bed reactors introduces mass transfer limitations.

X-ray diffraction (XRD) has been widely used for the purpose of phase identification in CaO based CO₂ sorbents. Li *et al.*^{34,35} for example, used XRD to determine the presence of mayenite (Ca₁₂Al₁₄O₃₃) in synthetic CaO based sorbents. Phase changes from CaO to CaCO₃

have also been identified by collecting dolomite aliquots at different times on stream during steam reforming coupled with *in situ* CO₂ capture.³⁶

When XRD is combined with Rietveld refinement it is possible to retrieve further information such as the magnitude of microstrain and crystallite size with crystallite being defined as a region with a continuous crystal lattice, and a particle as a collection of crystallites. Montez-Hernandez *et al.*³⁷ carried out XRD on Ca(OH)₂ particles that had been carbonated at different pressures. They were able to show a correlation between carbonation pressure and crystallite size from the XRD results using Rietveld refinement. Koirala *et al.*³⁸ compared CaO doped with different levels of Zr. A CaZrO₃ phase was identified which exhibited a larger crystal diameter with a higher level of Zr doping. Xu *et al.*³⁹ carried out XRD analysis of CaAl-layered double hydroxides synthesised using an ethanol/water mixture of varying ratios. The full width at half maximum (FWHM) of the (002) and (004) diffraction peaks were then used to calculate the crystallite size in the c-direction using the Scherrer equation.⁴⁰ This way they were able to show a correlation between ethanol to water volume ratio and crystallite size. Detailed information on differences in crystallite size in the different phases of dolomite samples heated to temperatures of 550 to 850 °C has been retrieved from the study of peak broadening.⁴¹ This could then be used to explain observations made during dolomite decomposition using TGA.

In situ XRD analysis is a technique which has been used to study phase changes⁴²⁻⁴⁴ decomposition⁴⁵⁻⁴⁷ as well as crystal size and strain effects^{48,49} in both CaO based materials and other materials such as perovskites and ternary oxides. Lucas *et al.*⁴³ used *in situ* XRD to study the effects of heating on CaCO₃. They were able to show a phase change from aragonite to calcite at a temperature of 450 °C. Efimov *et al.*⁴² used *in situ* XRD to show that BaCO₃ was formed in a two phase perovskite when it was heated to 900 °C in 50% CO₂ /50% N₂. By carrying out multiple XRD scans and analysing the resulting diffraction patterns using Rietveld analysis, they were able to plot the BaCO₃ fraction as a function of time. Liu *et al.*⁴⁴ studied phase changes in a synthetic two phase material containing CaO and Ca₁₂Al₁₄O₃₃. The amount of CO₂ around the sample was increased from 0 to 50 vol% at a constant temperature of 750 °C and the formation of a CaCO₃ phase was observed. By quantifying the three phases using Rietveld refinement Liu *et al.*⁴⁴ were able to show that the CaO converted to CaCO₃ while the Ca₁₂Al₁₄O₃₃ phase remained inert.

García-Martínez *et al.*⁴⁶ studied the decomposition of sulphated Ca(OH)₂ using XRD, and observed formation of CaO derived from Ca(OH)₂ beginning at 400 °C with no Ca(OH)₂ left at 600 °C, in addition to the formation of CaSO₄ and CaS from CaSO₃ which had formed

during sulphation. Engler *et al.*⁴⁵ examined the decomposition of dolomite in CO₂ and in air, and provided detailed descriptions of both decomposition mechanisms. They observed that in a CO₂ atmosphere dolomite first decomposes to CaCO₃ and MgO at 500-765 °C with a subsequent decomposition of CaCO₃ to CaO at temperatures above 900 °C. In an air atmosphere the dolomite first decomposed to CaCO₃, MgO and CaO at 700 - 750 °C followed by decomposition of the CaCO₃ to CaO at around 780 °C. Vieille *et al.*⁴⁷ used *in situ* XRD to study the decomposition of [Ca₂Al(OH)₆]Cl·2H₂O and compared it to TGA mass loss curves. The TGA results showed mass loss at temperature intervals of 25-280, 280-400 and above 400 °C, which was in agreement with the phase changes and changes in peak intensity observed by XRD in the same temperature intervals.

Rodriguez *et al.*⁴⁹ and Fernández-García *et al.*⁴⁸ combined XRD with Rietveld refinement to measure crystallite size and strain in mixed metal oxides and Ceria based ternary oxides respectively. Diffraction patterns were collected at different temperatures, and the crystallite size and strain were calculated from the width of the diffraction peaks. In addition to size and strain effects, Rietveld refinement can also be used for quantitative phase analysis. Hill and Howard⁵⁰ introduced a method for using the scale factors derived from Rietveld refinement to quantify the weight percentage of each phase in a chromatogram. They tested the method using TiO₂ and Al₂O₃ mixtures of known compositions and reported a relative error of 1-2%. Mixtures containing poorly crystalline phases however caused an error of 6.8%. Bish and Post⁵¹ and Kontoyannis and Vagenas⁵² used quantitative phase analysis to measure the wt% of mineral mixtures with known compositions and reported that the analysis had a relative error of 0.2-5.4%. Such an analysis provides the basis for studying the formation and/or decomposition of CaCO₃ and Ca(OH)₂ in a CaO based material during CO₂ capture in the presence of steam, or during surface area regeneration by hydration.

The motivation of the work presented here is to combine *in situ* XRD analysis with Rietveld refinement to investigate CO₂ capture of CaO based materials at temperatures between 25 and 800 °C, and to determine the mechanism of carbon capture in this commercially important system. The results are compared to those derived using TGA.

2 Results

2.1 CaO

Fig. 1 shows the XRD data, along with the modelled curve generated by Rietveld refinement and residual for CaO at 25 °C and 800 °C in a CO₂ atmosphere. A number of data

points are omitted in the figure (but not in the refinement calculation) to allow the solid line from the model to be observed clearly. In the upper trace at 25 °C, the data can be indexed to pure CaO (International Centre for Diffraction Data, ICDD, reference 037-1497). At 800 °C, however, additional peaks are observed which match with CaCO₃ in the calcite form (ICDD ref 007-0049). It is important to note from the flat nature of the base lines in Fig. 1 that there is no evidence of amorphous materials. Amorphous materials can be determined from XRD via the presence of extremely broad diffuse scattering.^{47, 53, 54} The quality of the refinements can be gauged using the residual, which is the difference between the model and the data (Fig. 1). Ideally, this line would be zero at all points, indicating that the model exactly matches the raw data, but this is extremely difficult to achieve in practice. Small deviations appear around some of the peaks, some of which are due to experimental scatter. This could be improved with extended scan times; hence there is a trade-off between maintaining data quality and minimising scanning time.

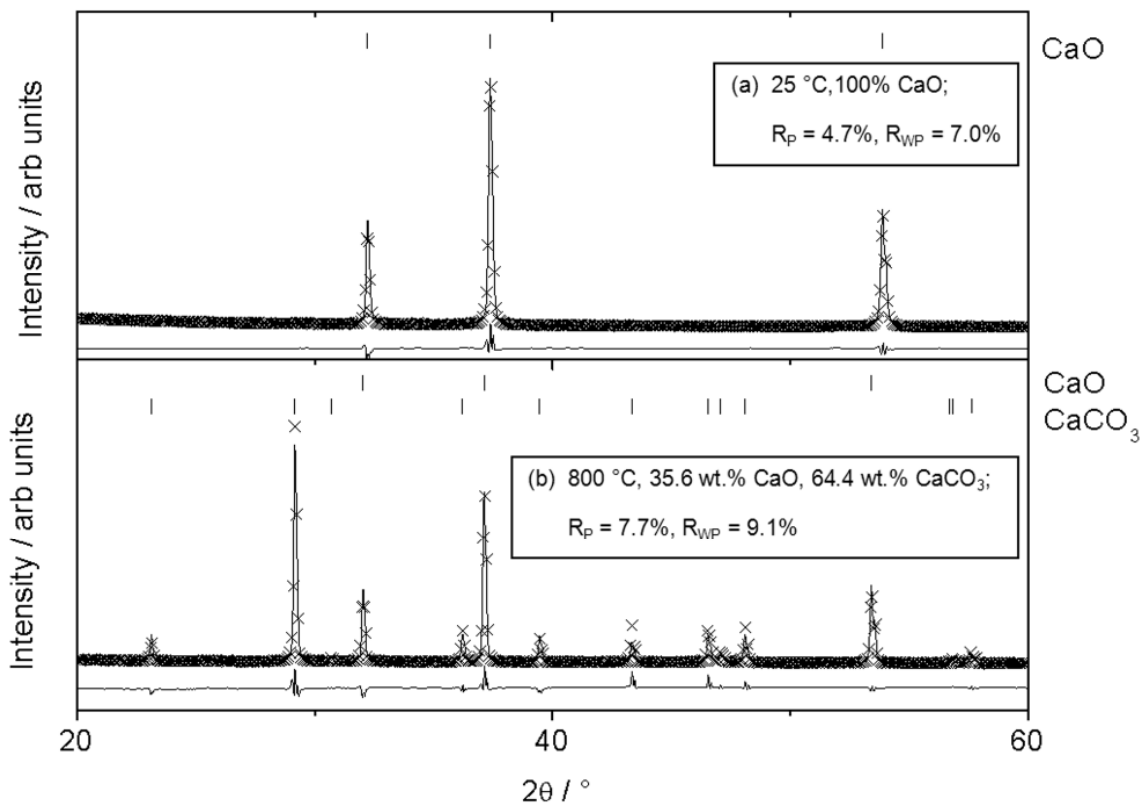


Figure 1. XRD spectra using CaO in a CO₂ atmosphere at (a) 25 °C and (b) 800 °C. Crosses = raw data, upper solid line = refinement model, lower solid line = residual. Insert showing phase composition (in wt%), residual (R_P) and weighted residual (R_{WP}). Vertical lines show the expected positions of diffraction peaks for CaO and CaCO₃.

The values of the residual (R_P) and of the weighted residual (R_{WP}) are a means by which to arithmetically gauge the quality of the fit.^{55,56} Values of 10% and below are considered typical for XRD data⁵⁷ so the values reported here (4.7-9.1%) are satisfactory.

From a refinement of the concentration of the various phases in the crystallographic model, we can determine the concentration of each phase in a mixture as a function of temperature (Fig. 2, where the XRD data is shown alongside that of the TGA for comparison). Note that in both the XRD and TGA data, the wt% of CaCO_3 is plotted, for ease of comparison and both 2 and 10 mg of sample were used in TGA to enable investigation of diffusion effects. Both the TGA and XRD data follow the same form of curve with XRD displaying a conversion in between those of TGA with 2 and 10 mg of sample. Sample mass had a significant impact on the conversion in the TGA system. This was attributed to diffusion limitations which increase with increasing sample mass in the TGA system. At 800 °C, TGA data shows a value of 53.3 and 71.8 wt% for 10 and 2 mg respectively while XRD provides a value of 64.4 wt%. The conditions used in this work differ from those used conventionally for TGA, to allow for a direct comparison to XRD data, in that XRD requires significantly longer scanning times at a particular temperature and this results in long carbonation times (14h in total for each experiment). However taking the conversions at 700-800 °C for example, the observed values fall within the spread of anticipated values from the literature.^{28,58,59}

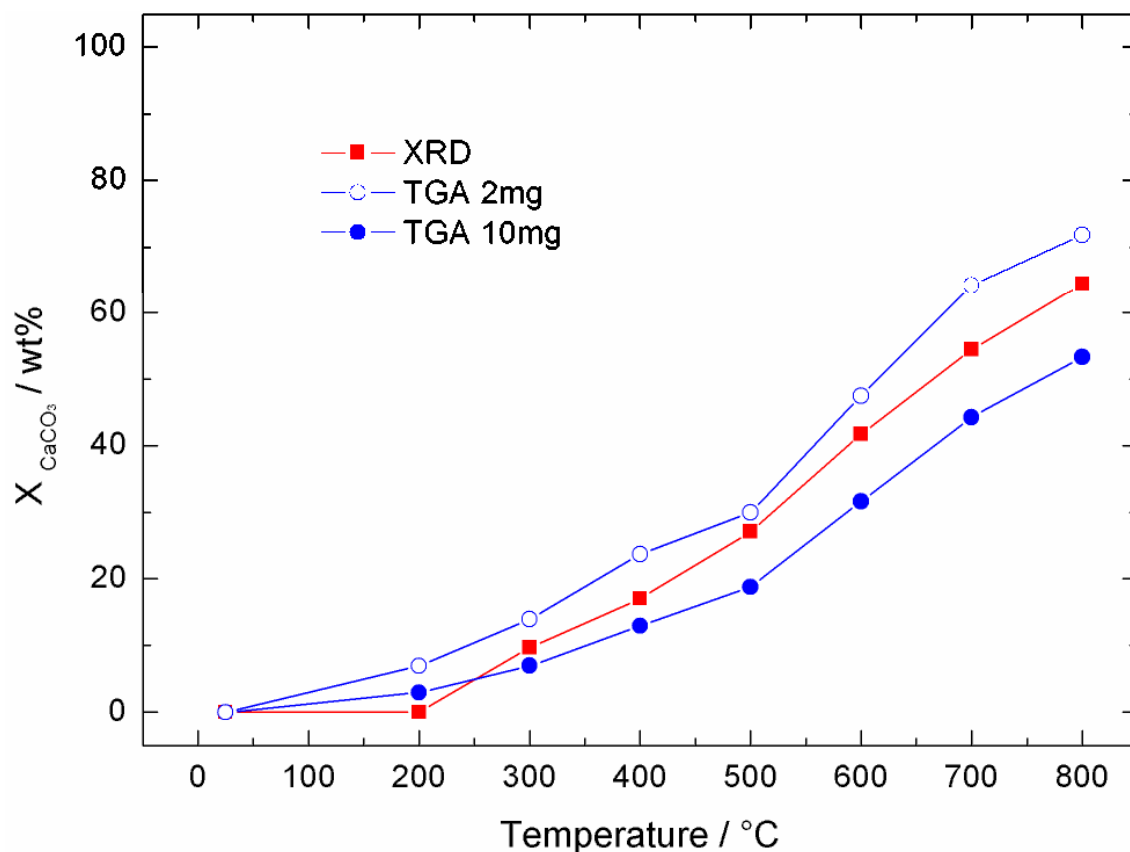


Figure 2. Conversion to CaCO₃ from CaO in a CO₂ atmosphere as a function of temperature, using XRD and TGA. Both are calculated as wt% CaCO₃.

2.2 Ca(OH)₂

Fig. 3 shows the XRD results for Ca(OH)₂ at 25 °C (Fig. 3a) and 800 °C (Fig. 3b), along with associated Rietveld refinements and residuals. At 25 °C the material was predominantly Ca(OH)₂, as anticipated (ICDD ref. 006-9147), but with a small amount of CaCO₃ which perhaps points to the high reactivity of the hydroxide to ambient CO₂. The refinement returned a value of 3 wt% for the CaCO₃ phase with R_P and R_{WP} values of 5.6 and 6.6 respectively. Following this observation the TGA calculations were amended to account for the 3 wt% CaCO₃ present in the Ca(OH)₂ at 25 °C (see Section 5). Note that there is considerable broadening of the diffraction peaks visible in Fig. 3(a). An analysis of this broadening using the size/strain algorithm in the software package used (X'Pert Highscore Plus) indicated that this was a combination of both size and strain broadening; size = 96 nm, and strain = 0.082%. This could be attributed to the hydration process described in Section 5. Considerable strain and size effects have been observed elsewhere from neutron diffraction studies of Ca(OD)₂, where D is deuterium.⁶⁰

Data collected at 800 °C showed a transformation to 100 wt% CaCO₃ (Fig. 3(b)) (ICDD ref. 04-007-0049). The broadening of these peaks was entirely instrumental, that is, strain and size broadening were absent.

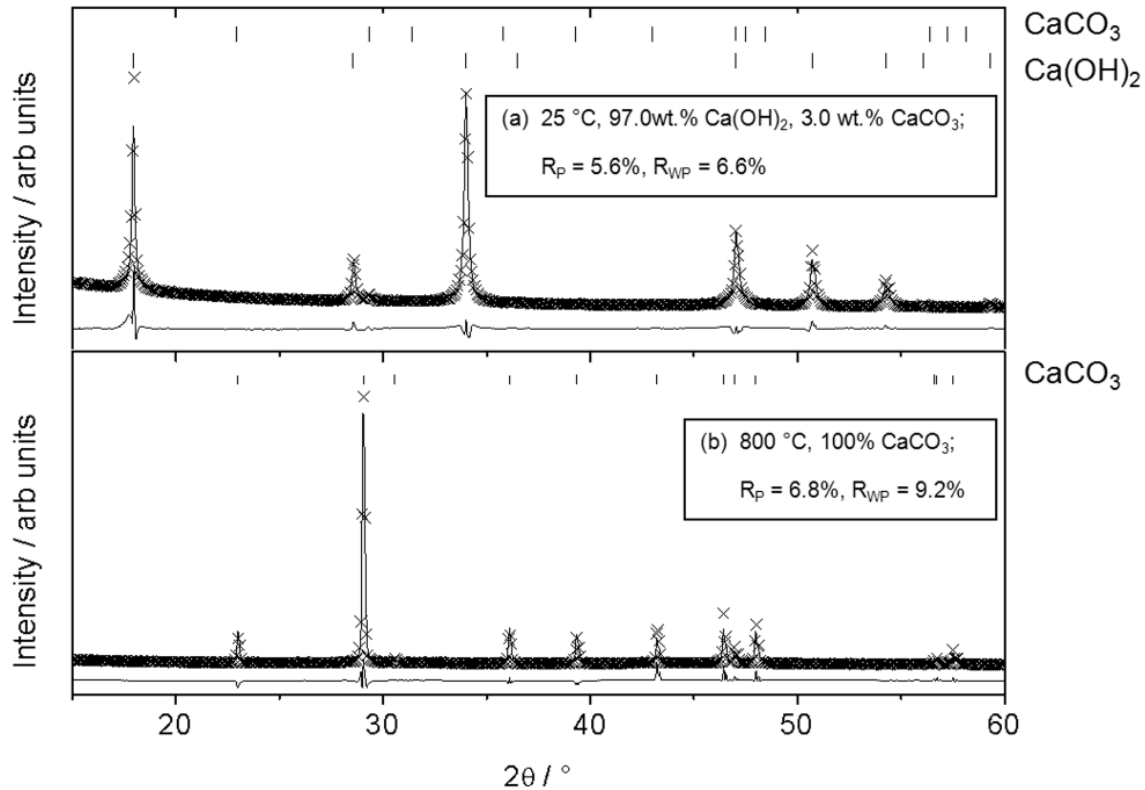


Figure 3. As Fig. 1 using Ca(OH)₂. Vertical lines show the expected positions of diffraction peaks for Ca(OH)₂ and CaCO₃.

The conversions of Ca(OH)₂ to CaCO₃ as functions of temperature determined by XRD and TGA are shown in Fig. 4. The profiles of the two data sets are close and while XRD shows complete conversion to CaCO₃ at 800 °C, TGA indicates a conversion to 94.3-96.4 wt% CaCO₃. Note that Ca(OH)₂ initially contained 3 wt% CaCO₃ according to the XRD analysis. This was expected as Ca(OH)₂ readily reacts with CaCO₃ at room temperature.²⁵ Therefore the wt% CaCO₃ was set to 3 at 25 °C for calculation of the conversion from TGA (see Section 5).

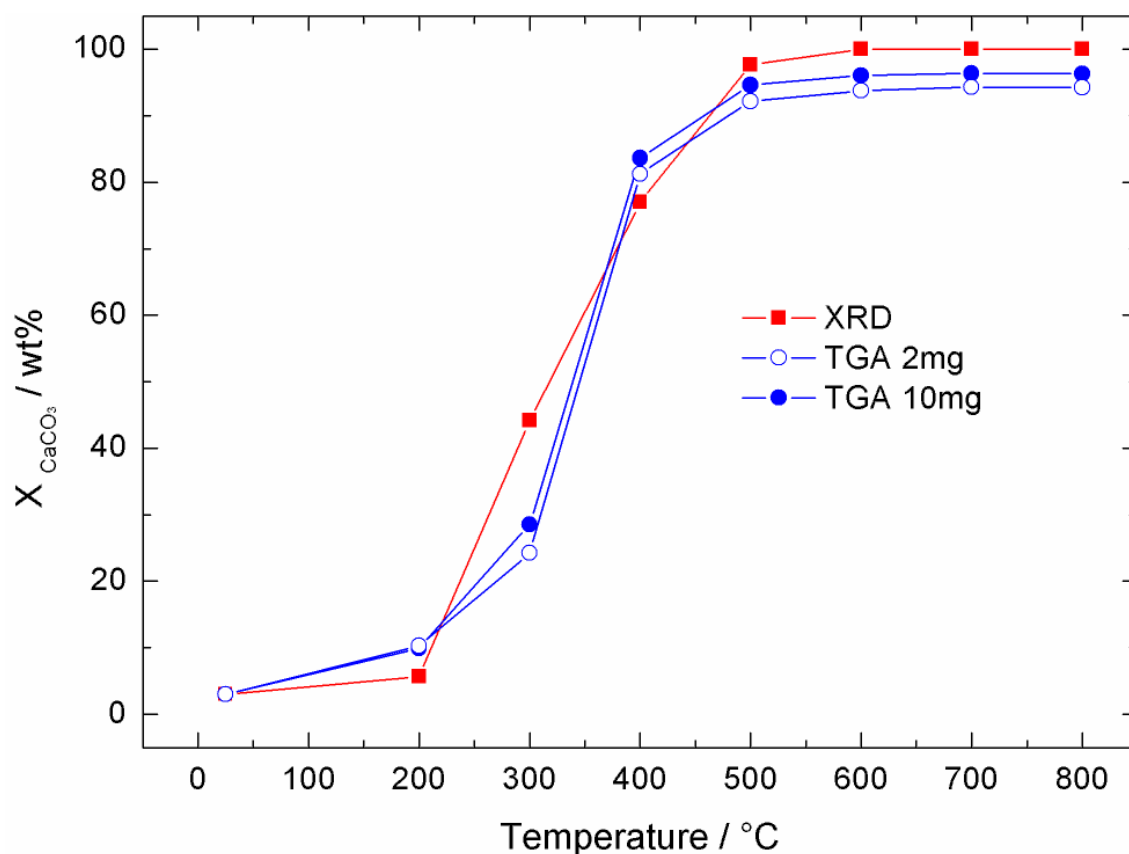


Figure 4. Conversion to CaCO_3 from $\text{Ca}(\text{OH})_2$ in a CO_2 atmosphere as a function of temperature, using XRD and TGA. Both are calculated as wt% CaCO_3 .

$\text{Ca}(\text{OH})_2$ reached a far higher level of conversion than CaO . The differences in conversion between $\text{Ca}(\text{OH})_2$ and CaO are in agreement with earlier work by Wu et al.⁶¹ and has been attributed to the increased surface area which is derived from hydration of CaO .^{19, 27, 28} Indeed, the B.E.T. surface area of the CaO and $\text{Ca}(\text{OH})_2$ were 3.5 and 24.9 $\text{m}^2 \text{g}^{-1}$ respectively (see supplemental information). However the difference in conversion may not be attributed to a difference in surface area alone since $\text{Ca}(\text{OH})_2$ has been shown to be more reactive towards CO_2 than CaO .^{31,32} Sample mass had no impact on the conversion of $\text{Ca}(\text{OH})_2$ in the TGA system which was attributed to lower diffusion limitations due to its high surface area.

Fig. 5 shows collected XRD data for increasing temperatures during the carbonation of $\text{Ca}(\text{OH})_2$. The material transformed from predominantly $\text{Ca}(\text{OH})_2$ at 25 °C to pure CaCO_3 at 800 °C. It is important to note that the transformation did not proceed via an oxide intermediate, that is, $\text{Ca}(\text{OH})_2$ converted directly to CaCO_3 . Short lifetime intermediates may have formed and then been removed, however these were not detected within the timescales of the XRD measurements. The approximate location of diffraction peaks derived from a

CaO phase (the positions would change with temperature) are shown on the x-axis in Fig. 5, at $2\theta \sim 32.2$ and 37.7° , but no peaks were observed at these diffraction angles.

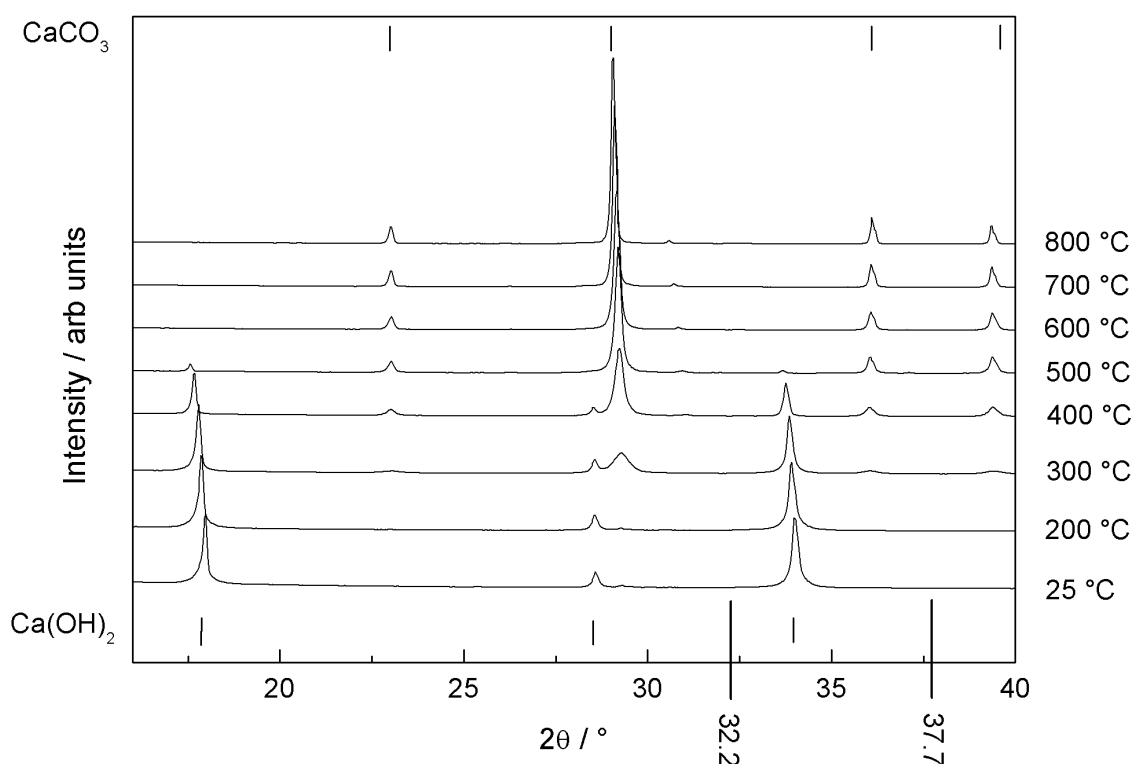


Figure 5. XRD spectra of Ca(OH)_2 transforming to CaCO_3 as a function of temperature. The location of CaCO_3 and Ca(OH)_2 diffraction peaks are shown via tick marks at the top and bottom respectively. CaO phase was not detected as an intermediate phase (absent peaks at $2\theta \sim 32.2$ and 37.7°).

2.3 XRD Calibration

In view of the minor disparity presented above between XRD and TGA, a rigorous calibration of the XRD method was conducted, using identical machine settings, such as irradiated area, collection times etc. This was performed by mixing known amounts of Ca(OH)_2 and CaCO_3 together, and the resultant mixtures were analysed using XRD, with subsequent Rietveld analysis. The CaCO_3 was prepared by heating Ca(OH)_2 (according to Section 5) to 700°C in a pure CO_2 atmosphere using a quartz reactor and a tube furnace. A gas flow of 50 ml min^{-1} was maintained in the quartz reactor using a mass flow controller (MKS, UK). This method relied on XRD only to confirm full conversion to CaCO_3 . Note that the CaCO_3 produced from the Ca(OH)_2 prepared here was in calcite form (Section 3.1), while commercially available high purity CaCO_3 powders contain mixtures of different forms, *e.g.* calcite and aragonite. It is possible to produce a pure calcite phase by heating to 600°C ⁴³ but

performing this on a commercially available CaCO_3 involves the same reliance on XRD. In addition, CaCO_3 prepared as above was more relevant to the experimental work and was hence used for the calibration. For each mixture, a total of 2 g was weighed (*e.g.* in the case of the 50/50 mixture 1 g of Ca(OH)_2 prepared according to Section 5, and 1 g of CaCO_3 were used). The Ca(OH)_2 and CaCO_3 were mixed using a pestle and mortar thus simultaneously crushing the mixture to a fine powder.

The results showed excellent correlation between the intended and measured compositions of the two phases, indicating that, at least in the case of a conversion from Ca(OH)_2 to CaCO_3 , the XRD refinement results were accurate (Table 1). It should be noted that pure Ca(OH)_2 was not achieved as the XRD analysis revealed the presence of 3 wt% CaCO_3 in the sample which was intended to be pure Ca(OH)_2 . Due to the extremely hygroscopic nature of CaO , it was not realistic to calibrate in this way for an intended CaO/CaCO_3 mixture. Rietveld analysis has been shown elsewhere to provide a reliable means of determining the phase concentration in a crystalline mixture.⁵⁰⁻⁵²

Table 1. Calibration of XRD Rietveld analysis. The listed measured values refer to the wt% values returned by the Rietveld refinement and the R_P and R_{WP} values for each refinement are also listed.

Intended composition (wt%)		Measured composition (wt%)		Agreement indices from Rietveld refinement (%)	
Ca(OH)_2	CaCO_3	Ca(OH)_2	CaCO_3	R_P	R_{WP}
0	100	0.0	100.0	5.6	7.6
25	75	25.8	74.2	6.2	8.1
50	50	50.0	50.0	6.5	8.1
75	25	73.3	26.7	6.2	7.8
100	0	97.0	3.0	6.2	7.4

2.4 Partially hydrated CaO

As described earlier, a CaO/Ca(OH)_2 mixture was analysed. This material was fabricated by exposing CaO powder to air (further information in Section 5). Fig. 6 shows XRD data, with Rietveld analysis for 25 °C and 800 °C. At 25°C the sample contained CaO

(64.7 wt%), Ca(OH)_2 (33.6 wt%), and a small amount of CaCO_3 (1.7 wt%). At 800 °C the sample had converted to a mixture of CaO and CaCO_3 .

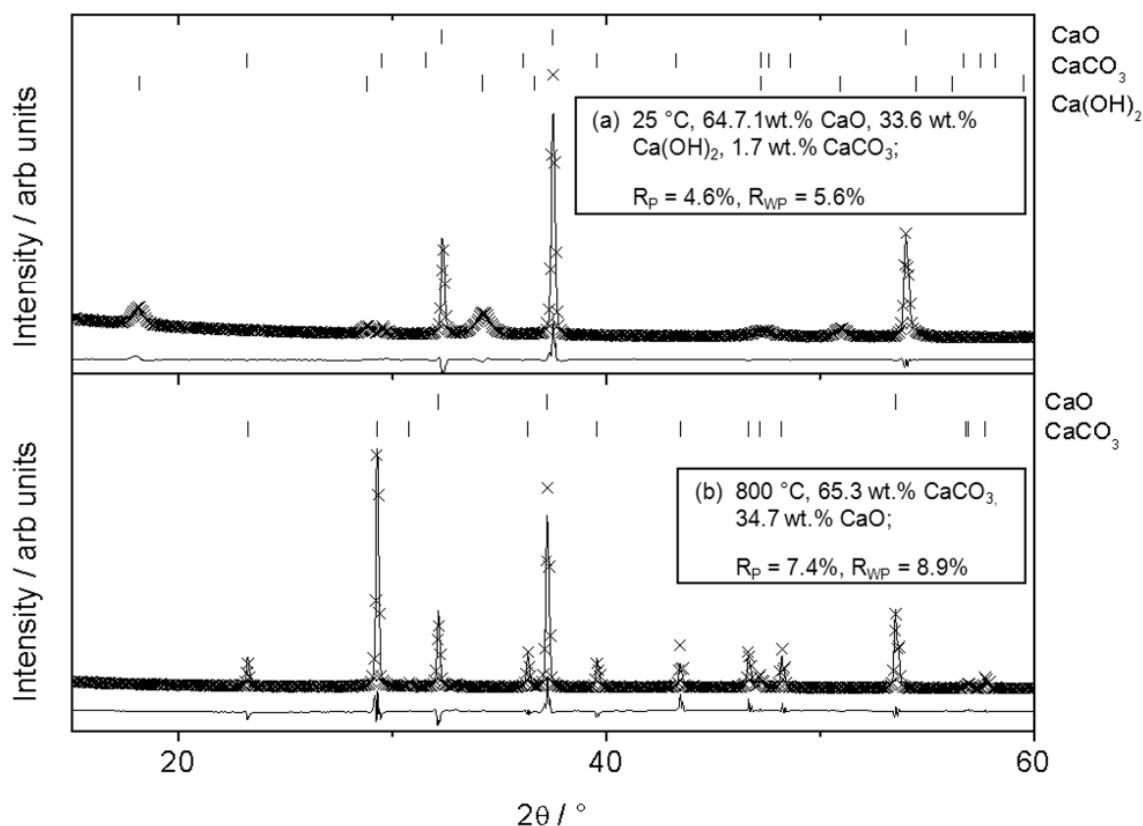


Figure 6. As Fig. 1 using partially hydrated CaO . Vertical lines show the expected positions of diffraction peaks for Ca(OH)_2 , CaO and CaCO_3 .

From an analysis of the peaks in Fig. 6(a) for the Ca(OH)_2 phase, there is evidence of anisotropic broadening, that is, some peaks were broader than others. Unfortunately, a thorough analysis of this anisotropic broadening was difficult using conventional XRD (*i.e.* Leeds apparatus) with the instruments used due to (i) significant instrumental broadening and (ii) the development of asymmetric peaks at low angles as a result of axial divergence, which is particularly problematic for $2\theta < 50^\circ$.⁶² To this end, high resolution synchrotron diffraction was conducted at the Diamond Light Source (Didcot, UK) on the mixed material at room temperature, the results of which are discussed in Section 3.5. This anisotropic broadening was evident from the XRD data collected at Leeds, with additional broadening for reflections resulting from (001) planes. This meant that reflections from the crystallographic *c*-axis were broader than those of the *a*-axis for the hexagonal Ca(OH)_2 . Such an effect has been observed elsewhere.⁶⁰

Fig. 7 shows the results of phase analysis from the refinement of the XRD data as a function of temperature. At temperatures above 300 °C, the concentration of Ca(OH)_2 rapidly diminished, and formed CaCO_3 in preference to CaO . It is important to note that although this sample contained significant amounts of Ca(OH)_2 , complete conversion to CaCO_3 did not occur; recall that for the pure Ca(OH)_2 , 100% conversion was possible, whereas for this mixture, containing 33.6 wt% Ca(OH)_2 only 65.3% conversion was reached.

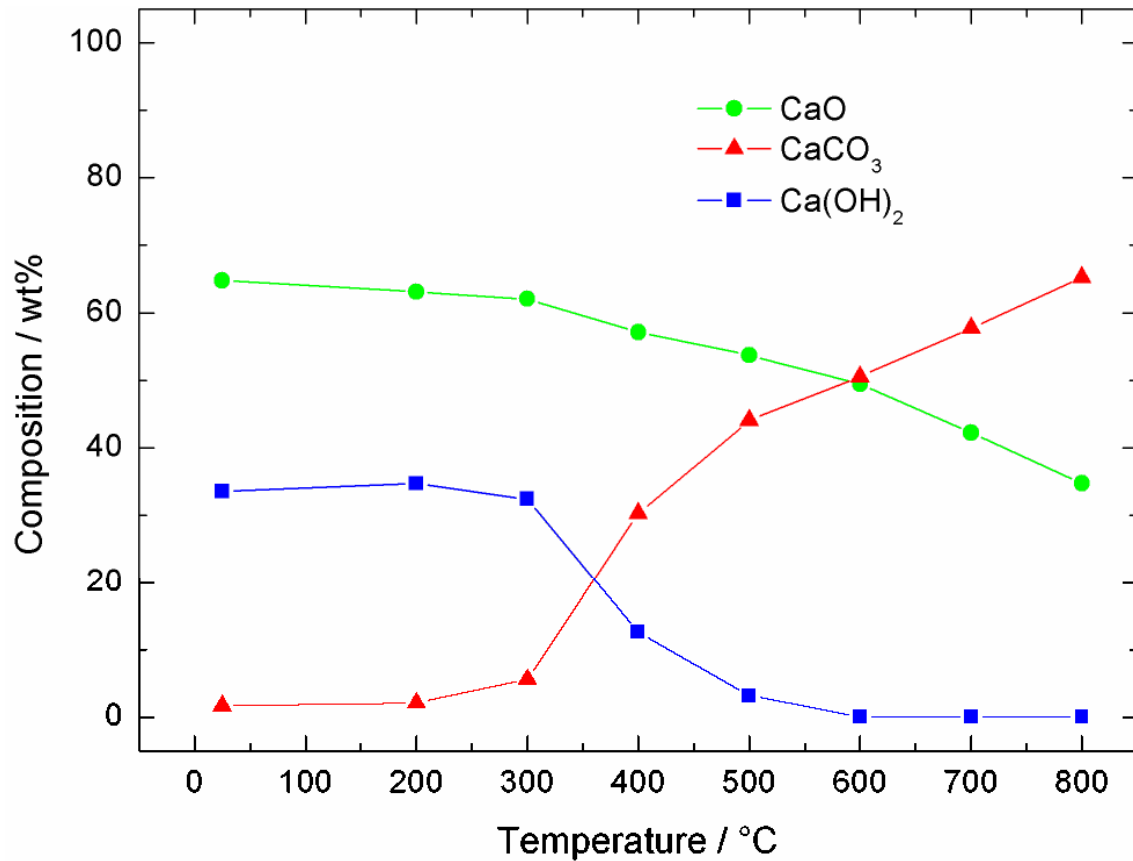


Figure 7. Composition of partially hydrated CaO in a CO_2 atmosphere as a function of temperature, as determined using XRD coupled with Rietveld refinement.

A comparison between XRD and TGA results is not shown here. TGA is unable to differentiate between the species responsible for the loss or gain of mass. Note that from the XRD data it can be concluded that CaCO_3 was formed through Reaction 2 between 300 to 600 °C and through Reaction 1 above 600 °C (Fig. 7). The principal problem posed by TGA as a technique of conversion analysis of partly hydrated CaO is that the sample contains two phases below 300 °C (CaO and Ca(OH)_2), 3 phases between 300 and 600 °C (CaO , Ca(OH)_2 and CaCO_3) and then two phases again above 600 °C (CaO and CaCO_3). This highlights a

strength of XRD analysis with Rietveld analysis, in that the wt% of multiple phases can be tracked during CO₂ capture.

At 800 °C the partially hydrated CaO showed a conversion to CaCO₃ of 65.3 wt%, which was similar to that obtained from CaO at the same temperature (64.4 wt%, Fig. 2), thus indicating same capture capacity. Interpreting Fig. 7 in the light of the results from Fig. 5 indicates that the Ca(OH)₂ transformed readily to CaCO₃ between 300 and 500 °C, such that at 600 °C, the Ca(OH)₂ had been entirely converted to CaCO₃. With the disappearance of the fast reacting Ca(OH)₂ above 600 °C, the CO₂ capture rate slowed, as the temperature increased, resulting in a same total amount transformed at 800 °C for the CaO as for the partially hydrated CaO, above 600 °C, both the pure CaO (Section 3.1) and partially hydrated materials behaved in the same manner.

To summarise, the conversions to CaCO₃ calculated using the Rietveld method, are shown in Fig. 8 for the three materials. From this limited data, pure Ca(OH)₂ transformed to 100 wt% CaCO₃ while the CaO and the partially hydrated CaO (which contained 33.6 wt% Ca(OH)₂) exhibited the same extent of conversion. This indicated that a small concentration of Ca(OH)₂ (about a 1/3 by weight) was not enough to enhance the capacity over that of CaO.

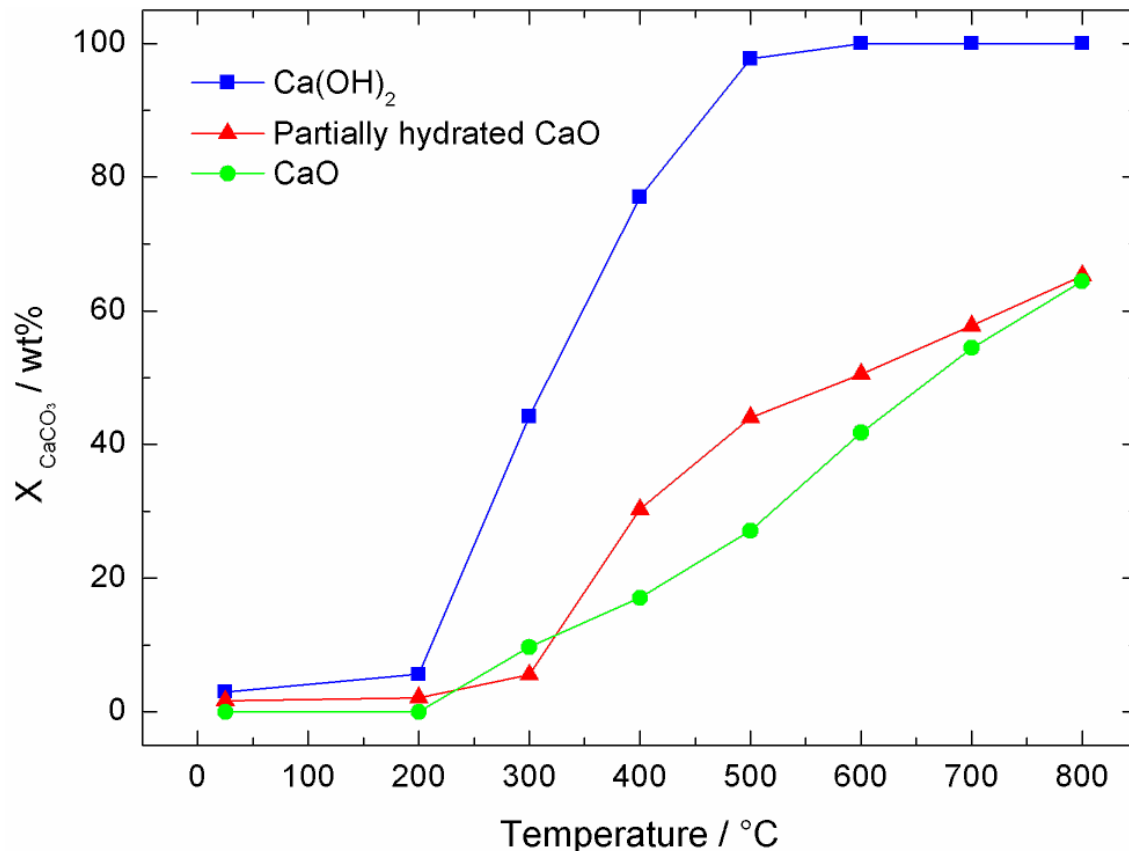


Figure 8. The wt% CaCO_3 in CaO , Ca(OH)_2 and partially hydrated CaO , as a function of temperature in a CO_2 atmosphere derived from XRD coupled with Rietveld refinement.

2.5 High resolution synchrotron diffraction

Partially hydrated CaO was studied at room temperature, in a sealed capillary tube, loaded in air. The data collected, along with the refinement and residuals are shown in Fig. 9. Note that a far larger range in diffraction angle, and d-spacing, was used for the refinements than reported in Sections 3.1-3.4. Moreover, the 2θ values were different compared to Figures 1, 3 and 6 as was the wavelength of the radiation used ($\lambda \sim 0.826 \text{ \AA}$, as opposed to $\sim 1.54 \text{ \AA}$ for $\text{CuK}\alpha$ radiation). The concentrations of the different phases determined using synchrotron diffraction were significantly different to those obtained from the XRD experiment at Leeds, with 74.1 wt% Ca(OH)_2 , 25.4 wt% CaO and 0.5 wt% CaCO_3 . Prior to analysis in the synchrotron, the powders had been sealed in a capillary using a flame from a micro-bunsen burner. This may have caused them to hydrate more, due a slight rise in temperature. Clearly, controlling the level of hydration of CaO during sample preparation would be extremely difficult.

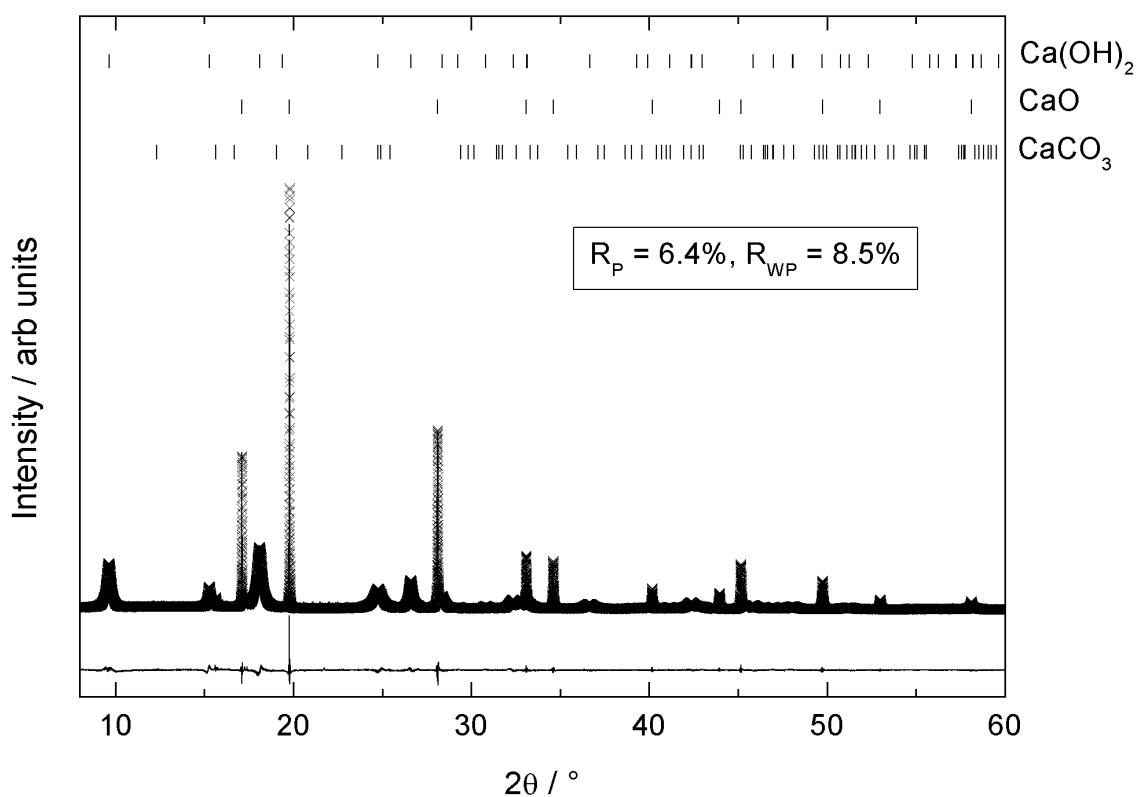


Figure 9. High resolution spectrum of partially hydrated CaO at room temperature, in a sealed glass capillary. Legend as Fig. 1.

A low angle range is plotted in Fig. 10, showing the significant broadening of the (001), (100) and (002) Ca(OH)_2 peaks. A CaO peak at $2\theta = 17.1^\circ$ is shown, which is extremely sharp. Note that, contrary to laboratory XRD, the characteristic instrumental broadening of I11 is extremely low. The (001) and (002) peaks were clearly broader than the (100) peak, and the full width at half maximum (β , or FWHM) are shown for each. Note from both Figs. 9 and 10, as was the case in the results from Section 3.4, that there was no evidence of amorphous material, as indicated by a flat baseline in the entire range $2\theta = 3\text{-}150^\circ$.

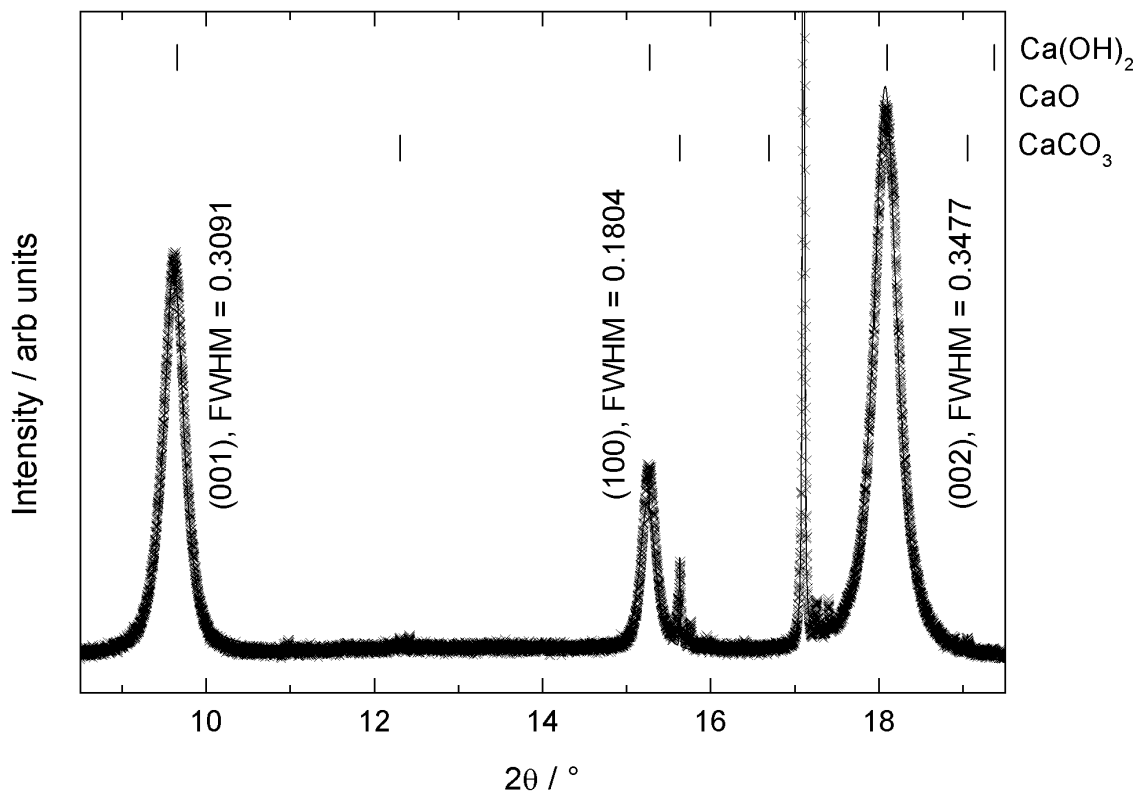


Figure 10. As Fig. 9 for 2θ range ($9\text{-}19^\circ$).

A number of parameters were altered during the structural refinement presented so as to correctly simulate the anisotropic broadening, prove the validity of the model, and calculate the phase content of Ca(OH)_2 . It was difficult, however, to determine the practical origin of this broadening from these refined parameters. Therefore, in order to quantify the anisotropic broadening, Williamson-Hall plots⁶³ were prepared (Fig. 11). Using this technique, $\beta\cos\theta$ was plotted against $\sin\theta$ for the (001) and (100) families. Then, via a determination of the gradient and intercept, and the instrumental broadening, the average microstrain and size effects (or coherence length) were determined respectively (Table 2).

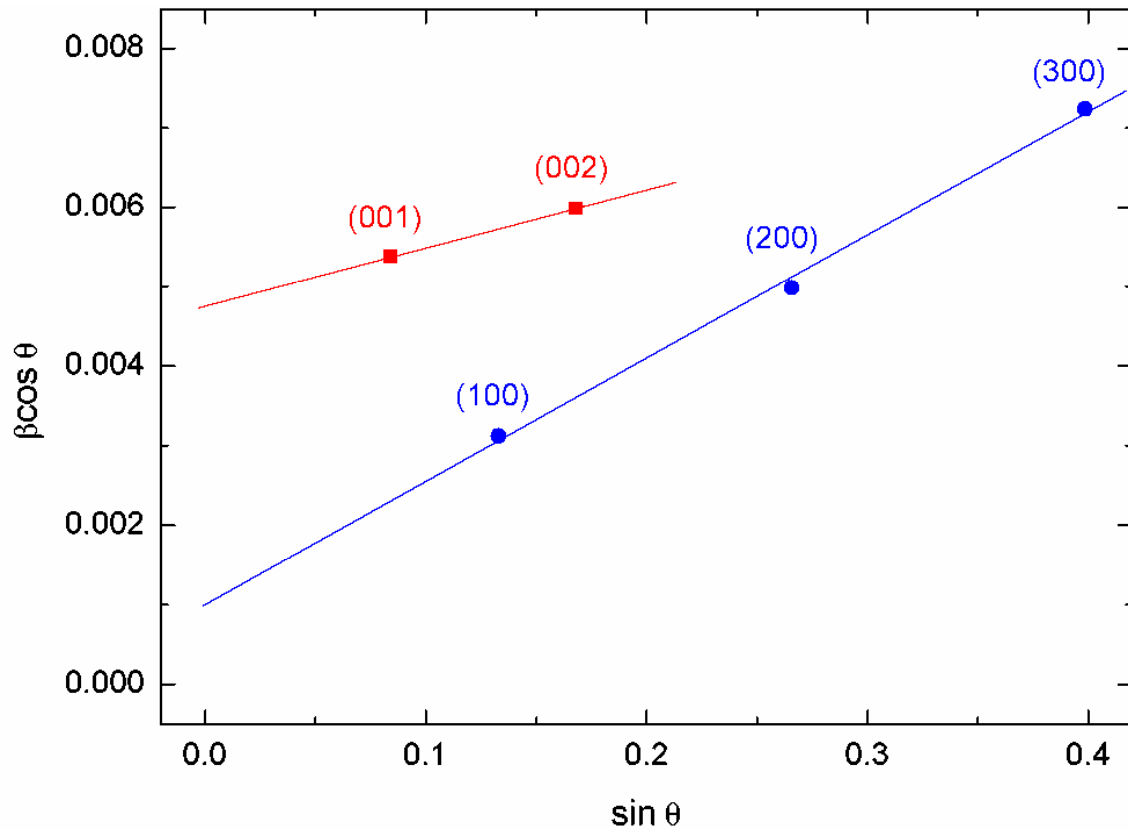


Figure 11. Williamson Hall plot for partially hydrated CaO, from data collected using high resolution synchrotron diffraction.

Table 2. Derived data from a Williamson Hall plot of high resolution synchrotron data of Ca(OH)_2 in partially hydrated CaO. For comparison, the derived strain, size and stress are also shown for pure Ca(OH)_2 , as determined using XRD at Leeds with subsequent Rietveld analysis.

	Slope	Intercept	Average strain / %	Size / nm	Stress / MPa
(001) direction	0.00722	0.00477	0.36	16	130
(100) direction	0.01551	0.00099	0.78	75	270
Pure Ca(OH)_2			0.082	96	29

In Table 2, there is a clear distinction between the crystallographic c and a axes, as determined from the different orientation-specific broadening. Crystal size and strain data could be interpreted, quite simply, as a highly strained Ca(OH)_2 shell, which formed around a CaO core (Fig. 12). The shell grew on the surface of a CaO core such that the (001) direction

(or the c-axis) of the $\text{Ca}(\text{OH})_2$ hexagonal phase was normal to the surface. From this analysis we estimate the thickness to be 16 nm, with an average microstrain of 0.36 %. Running parallel with the surface, a longer correlation length (or crystallite size) of 75 nm was determined. In this direction the average strain was almost double, at 0.78 %. The strain was expected to be highest in this direction, whereby interfacial clamping from the CaO core occurs. This clamping, or lateral stress is parallel to the surface and is due to the lattice parameter mismatch. The strain was lower normal to the surface of the core, as one of the faces of $\text{Ca}(\text{OH})_2$ was unconstrained.

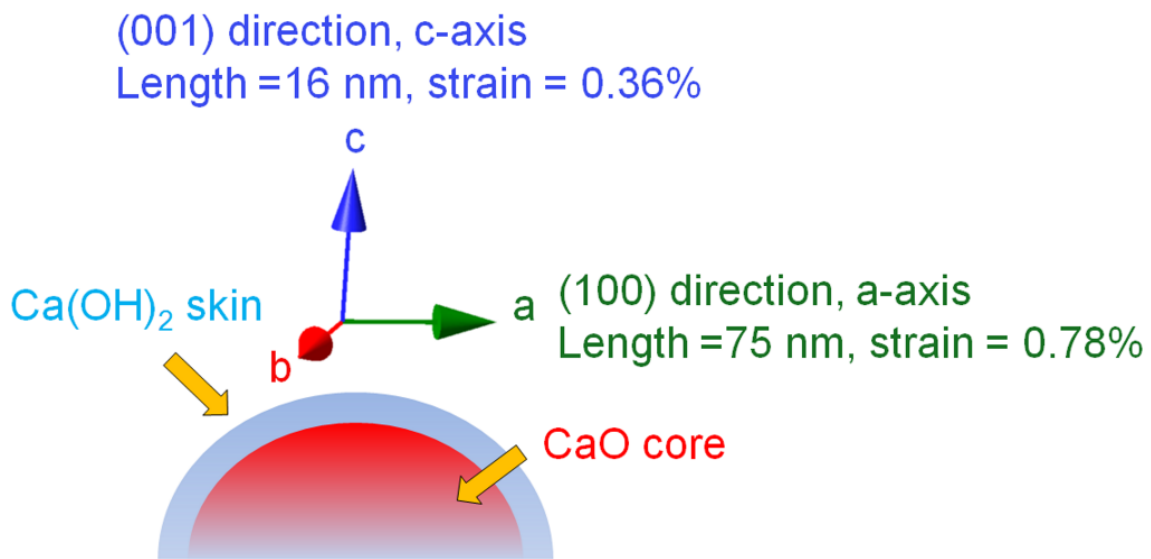


Figure 12. Schematic of a $\text{Ca}(\text{OH})_2$ shell forming on a CaO core in partially hydrated CaO, leading to extensive anisotropic broadening in diffraction peaks.

From the calculated strain values, and a knowledge of Young's modulus for the $\text{Ca}(\text{OH})_2$ phase (35.24 GPa⁶⁴), it was possible to estimate the average stress in the crystals (Table 2). This provides evidence of enormous internal stress, orders of magnitude higher than the yield strength of Portlandite, which explains the small crystal size. From data in the literature for porous Portlandite⁶⁴ a flexural strength of ca. 14-15 MPa can be extrapolated.

2.6 TEM

Transmission electron microscopy (TEM) was used to image the partially hydrated CaO precursor. A typical region is shown in Fig. 13. The materials studied were highly crystalline; lattice fringes were clearly visible and no amorphous regions were observed. Clear evidence of $\text{Ca}(\text{OH})_2$ crystallites were observed from this image. 75 crystallites were manually measured to give an average size of 83×16 nm (with a large standard deviation of

23 nm in length and 4 nm in width). This crystallite size was very close to that determined from the Rietveld refinement of synchrotron data presented in Section 3.3 (75×16 nm).

A Fourier transform of the lattice fringes indicated in Fig. 13 shows the existence of both CaO and Ca(OH)₂, providing evidence to corroborate the model stipulated in Fig. 12 of CaO coated with Ca(OH)₂, although a core-shell was not observed. Two different spacings were measured in the Fourier transform, one (ca. 0.26 nm) which corresponds to the (011) spacing of Ca(OH)₂ and the other (ca. 0.23 nm; indicated by arrows in Fig. 13) which corresponds to the (002) reflection of CaO.

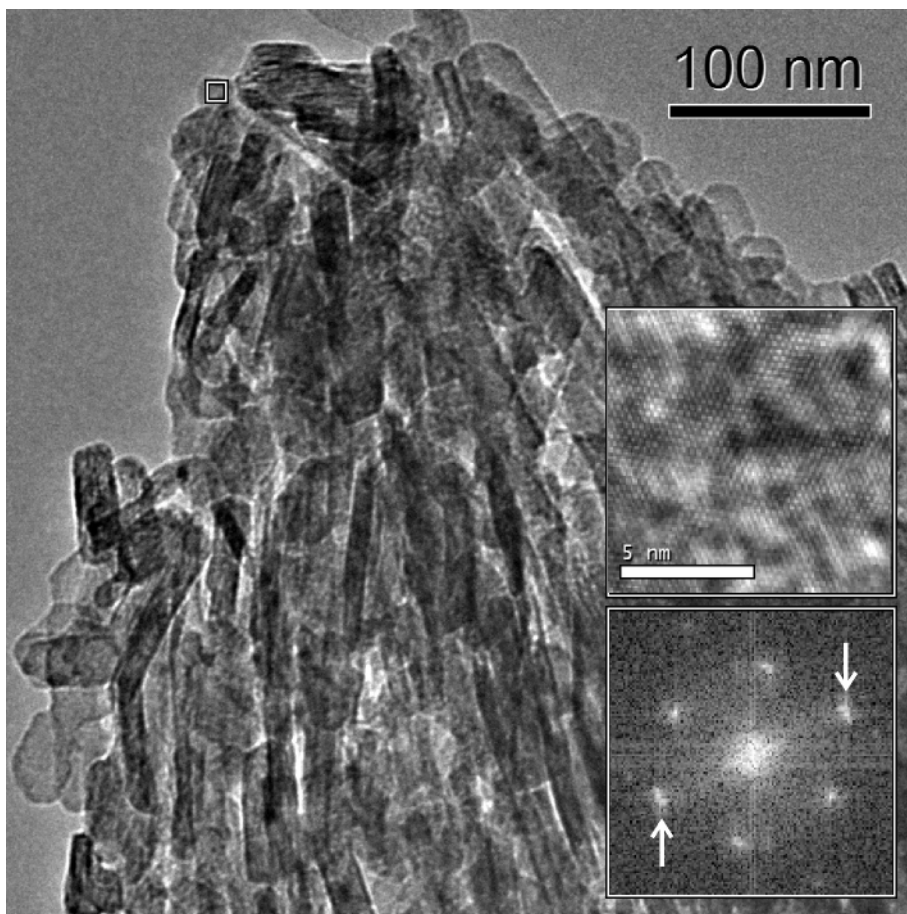


Figure 13. TEM image of platelets within partially hydrated CaO. Inserts (bottom right) show a lattice image and a Fourier transform of the region indicated by the small box (upper left). The arrows in the insert show the electron diffraction from CaO, the others are attributable to Ca(OH)₂.

3 Discussion

TGA has long been the mainstay for detailed studies into CaO based CO₂ sorbents, and will continue to be so. We present here *in situ* x-ray diffraction as a supplemental technique, by which the mechanism of capture and hydration can be determined.

Sample mass had a significant impact on the conversion of CaO in the TGA system which could be attributed to diffusion effects. Hence, the minor discrepancies between XRD and TGA results with regards to CaO could be attributed to differences in diffusion conditions between the two systems. However, there were also discrepancies between the XRD and TGA results with regards to Ca(OH)₂, and the likely origins of these are many.

1. The contact areas between sample and CO₂ were quite different in the TGA and XRD systems. The sample holders used were both cylindrical but with very different dimensions. The XRD sample holder had a cross section area of 250 mm² and a depth of 0.75 mm, whereas those of the TGA sample holder were 70 mm² and 2 mm, respectively. 2-10 and 220 mg of powder were used for TGA and XRD, respectively.
2. The flow of CO₂ past the samples was different. In the XRD setup at Leeds, the gas entered underneath the sample and flowed around it. However in the TGA setup the gas flowed from above the sample and was forced to flow upwards again after having made contact with the sample before continuing through the setup.
3. From an analysis of the XRD data, the phase fraction is explicitly known at any time; this is not the case in TGA, and the phase fraction may be quite different at each temperature, especially when the sample was a mixture of CaO and Ca(OH)₂.

In the case of Ca(OH)₂ conversion to CaCO₃, a thorough calibration of the XRD and Rietveld method strongly suggested the authenticity of the values presented, that is, transformation to 100% CaCO₃; peaks resulting from CaO and Ca(OH)₂ are absent. The difference in the capture capacity of CaO, and Ca(OH)₂ is well known and can be attributed both to differences in reactivity towards CO₂ and the increase in surface area induced by formation of Ca(OH)₂ via hydration of CaO.

A comparison of pure CaO and partially hydrated CaO (ca. 1/3 Ca(OH)₂ by weight) showed that both materials reached the same capture capacity, that is, at 800 °C both mixtures were 64.4-65.3 wt% CaCO₃. Undoubtedly the study presented here is limited, but regardless of the differences in composition, the capture capacity was the same. The pure Ca(OH)₂ material (which contained a very small fraction of carbonate) exhibited 100% conversion to

CaCO₃. It is possible, therefore, that a threshold Ca(OH)₂ concentration exists, above which total transformation to CaCO₃ can occur. Such a technical knowledge could play an important role in understanding the effect of hydration on CaO based CO₂ sorbents. This will form the basis of further work.

The mechanism for the formation of CaCO₃ from CaO has been reported extensively in the literature.^{18,19,24,58,65} As for the Ca(OH)₂ and CaO/Ca(OH)₂ mixture, we are only able to describe large correlated regions of the structure, as discussed earlier. We are, however, able to show that the Ca(OH)₂ phase of the mixture reacts with CO₂ to form CaCO₃, prior to the CaO phase and that capture of CO₂ from Ca(OH)₂ proceeds directly to CaCO₃ without the formation of a reaction intermediate as determined within the timescales of the XRD measurement. The form of the resulting CaCO₃ is calcite, as anticipated.

It is well known that hydration causes loss of mechanical strength in CaO based materials.^{26, 29, 30} In Section 3.5 and Table 2, we were able to determine size and strain for the Ca(OH)₂ crystallites at room temperature. The large microstrain provides a clear mechanism whereby the internal stress developed during hydration causes damage to CaO based materials; the interfacial stress generated by the marriage of CaO to Ca(OH)₂, viewed alternatively as diffusion of water into the CaO lattice, exceeds the rupture strength, leading to disintegration. The stress is far higher than in the pure Ca(OH)₂, which we propose is due to an interfacial coupling with CaO. For pure Ca(OH)₂, the strain is much lower, and the crystal size is larger (Table 2). The apparent stress for the pure Ca(OH)₂ was ca. 29 MPa, an order of magnitude lower than observed in the partially hydrated CaO. An analysis of the anisotropic peak broadening points to a mechanism whereby hydration leads to catastrophic failure in these materials, via the generation of stresses of around 20 times the strength of Ca(OH)₂. Microstrain was also observed in the CaCO₃ phase during CO₂ capture with the pure CaO material investigated in Section 3.1 (see supplemental information). However this microstrain was initially ca. 0.4% at 300-400 °C, i.e. far lower than that observed for the Ca(OH)₂ phase in the partially hydrated CaO (0.78%). The stress in the CaCO₃ then reduced with increased temperature and was nonexistent above 600 °C.

The high stresses that are induced, and the orientation of the Ca(OH)₂ phase can be understood by a consideration of the crystal structures for both CaO and Ca(OH)₂. CaO forms a simple cubic structure, and the arrangement of Ca atoms in the a-b plane form a square array, with a Ca-Ca bond length of 3.401 Å (as determined from the Rietveld analysis of synchrotron data). The structure of the hydroxide is more complex, and forms a hexagonal lattice (Fig. 14).

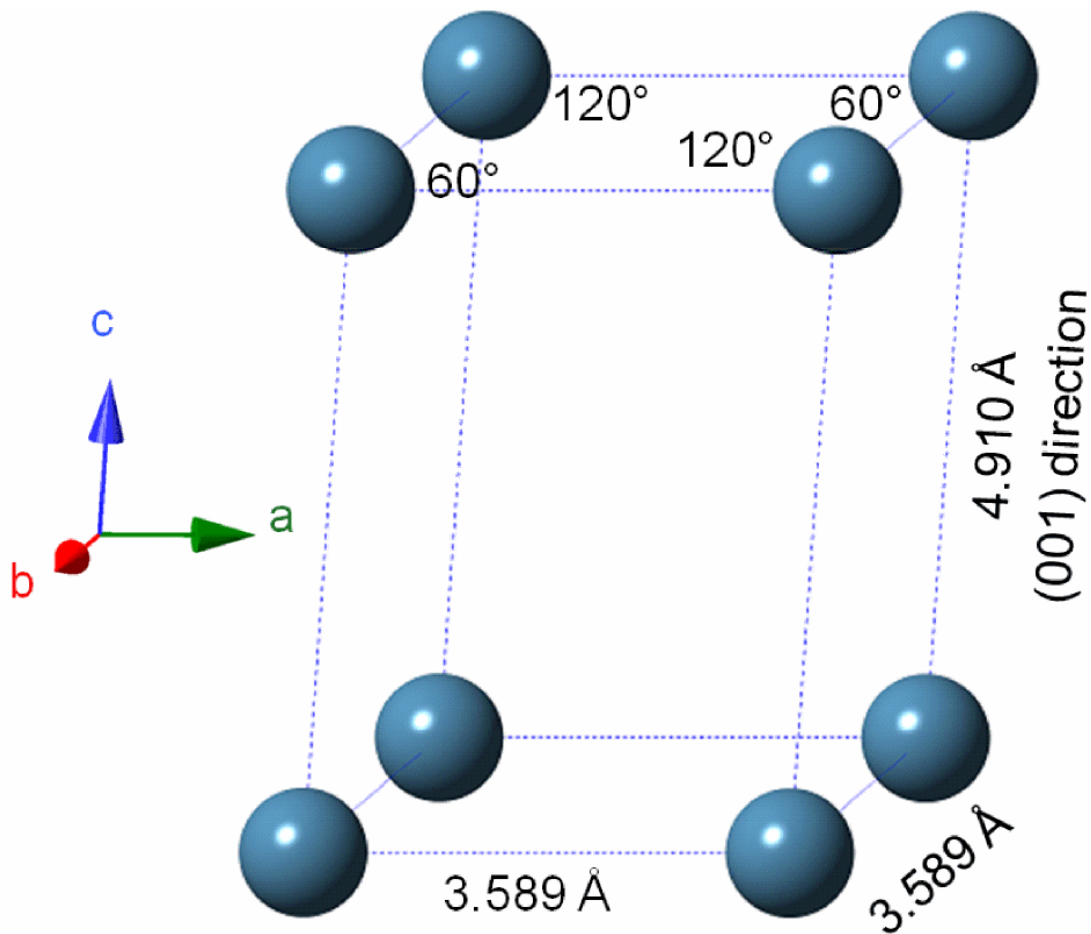


Figure 14. Simplified unit cell of hexagonal $\text{Ca}(\text{OH})_2$ lattice showing only Ca ions. Two distinct Ca-Ca bond lengths are apparent.

In Fig. 14 only the Ca ions are shown. There are clearly two Ca-Ca bond lengths, whereas in CaO there is only one. The length which most closely matches that of the CaO Ca-Ca bond is 3.589 \AA , hence the a-b plane of the $\text{Ca}(\text{OH})_2$ phase forms the interface with the CaO core, and the (001) direction, or the c-axis, is normal to the CaO/ $\text{Ca}(\text{OH})_2$ interface. There is, however, an extremely large mismatch between the a-b planes of the CaO and $\text{Ca}(\text{OH})_2$ arrays in terms of both the Ca-Ca bond length which differs by 5.5%, but also the fact that the Ca ions in CaO form a square lattice, whereas in $\text{Ca}(\text{OH})_2$ they are hexagonal in the a-b plane, with angles of 60 and 120° (Fig. 14). This leads to the large level on interfacial stress observed, and ultimately, disintegration.

Clearly, lattice mismatch is responsible for the large anisotropic stresses in $\text{Ca}(\text{OH})_2$, but not necessarily the high aspect ratio. The lattice matching is responsible for the orientation of the $\text{Ca}(\text{OH})_2$, with the c-axis normal to the CaO/ $\text{Ca}(\text{OH})_2$ interface. A

mechanism is presented below, whereby interaction with water vapour leads to a transformation from oxide to hydroxide.

1. Absorption of water molecule into CaO. Region of (001) orientated hydroxide forms on surface. The hydroxide seeds the formation of further hydroxide, potentially reducing the activation energy for further reaction.
2. The next molecule of water arrives and may (a) diffuse through Ca(OH)₂ and react with fresh CaO beneath the hydroxide or (b) react with CaO, adjacent to existing hydroxide on the surface.
3. Growth continues. From a steric viewpoint, growth of Ca(OH)₂ will proceed far more rapidly parallel to the CaO/Ca(OH)₂ interface, as the diffusion path for the reacting water is lower. For unconstrained Ca(OH)₂, there may be very different growth rates for the various facets, as is observed in a number of different systems (for example, ZnO⁶⁶), which when grown from solution/melt form high aspect ratio crystallites.
4. A highly oriented platelet form on the surface. The lattice mismatch between CaO and Ca(OH)₂ results in large levels of stress. Further growth leads to eventual rupture and formation of fresh CaO surface.

It is well known, and we confirm the same here, that Ca(OH)₂ transforms to CaCO₃ far more readily than CaO. In the system which contains CaO/Ca(OH)₂, and for other systems such as CaO/CaCO₃ the internal stress generated at the interface may well serve to increase the reactivity further by reducing the activation energy. Neglecting the changes in entropy and temperature, we can approximate the change in internal elastic energy per unit volume, ΔU , of the strained Ca(OH)₂ phase in the (100) direction, from the average microstrain ϵ_{100} and Young's modulus 'YM' ($\Delta U = \frac{1}{2} \text{YM} \times \epsilon_{100}^2 = 0.5 \times 35.24 \times 10^9 \text{ Pa m}^{-3} \times 0.0078^2 \text{ m}^2 \text{m}^{-2} = 1.072 \times 10^6 \text{ J m}^{-3}$). Multiplying DU by the molar volume for Ca(OH)₂ as calculated from the crystallite volume derived from the Rietveld refinement and Avogadro's number ($54.82 \times 10^{-30} \times 6.0221 \times 10^{23} = 3.301 \times 10^{-5} \text{ m}^3 \text{ mol}^{-1}$), we generate a value of internal energy change of ca. 35 J mol⁻¹. It seems unlikely, therefore, that this elastic energy, which is much lower than RT (where R is the gas constant, and T the absolute temperature) has much direct effect on the activation energy, which we estimate to be many kJ mol⁻¹.

XRD is only able to study relatively large bodies over long time periods, as myriad atoms are required in order to generate a diffraction pattern. The small crystallite of Ca(OH)₂ which we identified in Sections 3.5 (WH plots) and 3.6 (TEM), contains many atoms; a

cuboid of dimensions $16 \times 75 \times 75$ nm comprises 1.6 million formula units. In addition, the size and microstrain we calculate is an average of many crystallites of $\text{Ca}(\text{OH})_2$. It is therefore not possible to use XRD to probe the carbon capture mechanism or the reaction of CaO with water at the atomic level. In order to do this, other techniques such as *ab initio* calculations may be required.

It must be noted from the literature, that the structure of polycrystalline $\text{Ca}(\text{OH})_2$ is highly complex. As noted earlier, Chaix-Pluchery *et al.*⁶⁰ observed highly anisotropic peak broadening, which they attributed to trapping of protons by hydroxyl groups in (001) planes. Xu *et al.*⁶⁷ however, noted only a very slight anisotropic broadening from neutron diffraction of polycrystalline materials. Although the model above is plausible from the analysis of the synchrotron data, other factors may be partially responsible for the observed anisotropy, specifically, dislocations, stacking faults, twinning and of course, crystalline size anisotropy.⁶⁸

The materials studied here were in powder form, consisting of small particles and loss of mechanical strength has been observed in materials consisting of larger particles (400-710 μm) than the ones used here.^{26,29,30} The use of powders were necessary using XRD and consequently also when using TGA to enable direct comparison. Particle size has been shown to influence the mechanism of CO_2 capture and calcination in CaO based materials like for example effects regarding heat and mass transfer.^{32,69-71}

TEM analysis showed the presence of $\text{Ca}(\text{OH})_2$ crystallites nominally 83×16 nm in size, which compares well with the values calculated from synchrotron diffraction of 75×16 nm. The good agreement between these two very different methods provides strong evidence that the analysis of the anisotropic broadening is robust, and that the calculations of strain and stress presented here are also reliable. One must always consider, however, the difference in volumes probed by the synchrotron radiation and the TEM (Fig. 13), which differ by a factor of 10^{11} . CaO and $\text{Ca}(\text{OH})_2$ were however identified from Fourier transforms of selected areas in the TEM images.

4 Experimental

Three materials were fabricated in powder form for this study, specifically CaO, $\text{Ca}(\text{OH})_2$ and a mixture thereof resulting in CaO that was partially hydrated. CaO was prepared from commercially available CaO powder (99.95% purity, metal basis, Alfa Aesar) by heating the powder to 700 °C in a pure N_2 atmosphere immediately prior to the CO_2

capture experiments to remove Ca(OH)_2 impurities. This was conducted in both the TGA and XRD systems (see the respective sections on the TGA and XRD systems for further details). The CaO powder was heated to 100 °C then to 200, 300, 400, 500, 600 and 700 °C under a flow of N_2 (99.998% + minimum, oxygen free from BOC, UK) at a flow rate of 50 ml min^{-1} controlled by a mass flow controller (MKS, UK) with a 10 min hold at each temperature. The 10 min hold allowed for an XRD scan to be carried out at each temperature so that the removal of the Ca(OH)_2 could be monitored in the XRD system. The same temperature program was subsequently used in the TGA system to allow for direct comparison. The CaO powder was then cooled to room temperature in N_2 and the atmosphere was then switched to CO_2 (99.995 %, CP grade from BOC, UK) prior to data collection.

In order to prepare Ca(OH)_2 , 760 ml of deionised water was heated in a beaker on a hot plate and agitated with a magnetic stirrer. When 75 °C was attained, 130 ml of 2-propanol (CHROMASOLV Plus, HPLC grade, Sigma Aldrich) was added to the beaker together with 26.2 g CaO powder (99.95% purity metal basis, Alfa Aesar) and the resulting solution was stirred for 1h at 75 °C. The beaker was put in an oven overnight at 120 °C to evaporate the water from the solution. The residue was crushed to a fine powder using a pestle and mortar. This hydration method has been used previously by Li *et al.*^{34,35}

The partially hydrated CaO was untreated CaO powder (99.95% purity on a metal basis from Alfa Aesar). Since CaO is highly hygroscopic, Ca(OH)_2 readily forms from the CaO, such that the CaO powder contained 30-35 wt% Ca(OH)_2 after contact with air for 5 min.

TGA was carried out using an air cooled TGA 50 Shimadzu thermogravimetric analyser with an alumina crucible and a TA 60 thermal data acquisition package. The crucible had a cylindrical shape with a cross sectional area of 70 mm^2 and height of 2 mm. For every run, the crucible was taken out and cleaned, after which the system was tared with the cleaned crucible back in place. A mass of nominally 10 mg or 2 mg of sample was added to the crucible and the analysis was started. A blank run was carried out so that corrections for buoyancy effects could be made. The temperature was increased with a heating rate of 40 °C min^{-1} to 200, 300, 400, 500, 600, 700, and 800 °C with a 2h hold at each temperature and mass readings were logged every 30s. The temperature program was designed to enable a direct comparison with the *in situ* XRD results.

To allow for a simple comparison with XRD data, the TGA data was presented in wt% of the assumed CaCO_3 phase. The wt% CaCO_3 in the sample at any given temperature was derived from the sample mass (m_t , see Equations 1, 2 and 3) recorded at the end of each

2h hold. The wt% of each phase (CaO, CaCO₃ and Ca(OH)₂ from the XRD experiments was readily calculated using Rietveld refinement). TGA data is often presented in percentage conversion to CaCO₃ on a molar basis.^{18,59,72} In single phase samples such as CaO and Ca(OH)₂ this is comparable to wt% CaCO₃.

In the equations below, X_{CaCO_3} is the weight % of CaCO₃ in the reacting solid mixture, W is molar mass, m_t = mass reading at time t and m_i is the initial mass of either CaO or Ca(OH)₂. Note that the CaO samples contained pure CaO while the Ca(OH)₂ contained 3 wt% CaCO₃ (Table 1). Therefore m_i in the case of Equation 1 equals the initial mass reading while m_i in the case of Equations 2 and 3 is 97% of the initial sample mass reading to account for the presence of CaCO₃ at the start of the experiment. The wt% CaCO₃ was also set to 3 at 25 °C for the TGA results.

The wt% of CaCO₃ in the sample at any time via CaO carbonation (Reaction 1) is given by Equation 1:



$$\text{Therefore, } X_{CaCO_3}(t) = 100 \times \left(\left(\frac{m_t - m_i}{W_{CO_2}} \right) \times \frac{W_{CaCO_3}}{m_t} \right) \quad \text{Equation 1}$$

Similarly, the wt% of CaCO₃ in the sample at any time (for which temperature is below 400 °C), through reaction 2 is given by Equation 2:



$$X_{CaCO_3}(t) = 100 \times \left(\left(\frac{m_t - m_i}{W_{CO_2} - W_{H_2O}} \right) \times \frac{W_{CaCO_3}}{m_t} \right) \text{ (up to 400 °C)} \quad \text{Equation 2}$$

For calculation of the wt% CaCO₃ (X_{CaCO_3}) is assumed that any difference in mass at a given time from the starting mass is due solely to the formation of CaCO₃ by Reaction 1 in the case of CaO and Reaction 2 in the case of Ca(OH)₂ at temperatures below 400 °C and above it is assumed that all Ca(OH)₂ is decomposed to CaO and formation of CaCO₃ occur through Reaction 1.

$$X_{CaCO_3}(t) = 100 \times \left(\frac{m_t - \left(\frac{m_i}{W_{Ca(OH)_2}} \right) \times W_{CaO}}{W_{CO_2}} \right) \times \frac{W_{CaCO_3}}{m_t} \text{ (above } 400 \text{ } ^\circ\text{C)} \quad \text{Equation 3}$$

The partially hydrated CaO was not studied using TGA. This is discussed further in Section 3.4.

Evidence for CO₂ capture by Ca(OH)₂ through Reaction 2 was reported by Blamey *et al.*³² who observed simultaneous evolution of H₂O and increase in mass when studying Ca(OH)₂ samples using TGA-MS. Using TGA it has been shown that Ca(OH)₂ readily decomposes at temperatures above 400 °C in N₂ at such a rate that all Ca(OH)₂ could be assumed to have decomposed by the end of the 2h hold during the carbonation experiment carried out here.⁷³ This is in agreement with investigations of Ca(OH)₂ decomposition in the TGA system described above (see supplemental information for further details and discussion).

XRD data at Leeds was collected using a P'Analytical X'Pert MPD with compatible oven (HTK-1200 high temperature chamber, Anton Paar, Austria) with an alumina sample holder. The sample holder had a cylindrical shape with a cross sectional area of 250 mm² and a height of 1 mm. The full volume of the sample holder was filled with sample corresponding to a sample mass of ≈ 125 mg. To control the atmosphere, CO₂ or N₂ (same gases as used for TGA) were fed into the sample chamber at a rate of 50 ml min⁻¹ using mass flow controllers (MKS, UK). A Dreschel bottle filled with water was connected to the output of the chamber to monitor the flow (Fig. 15).

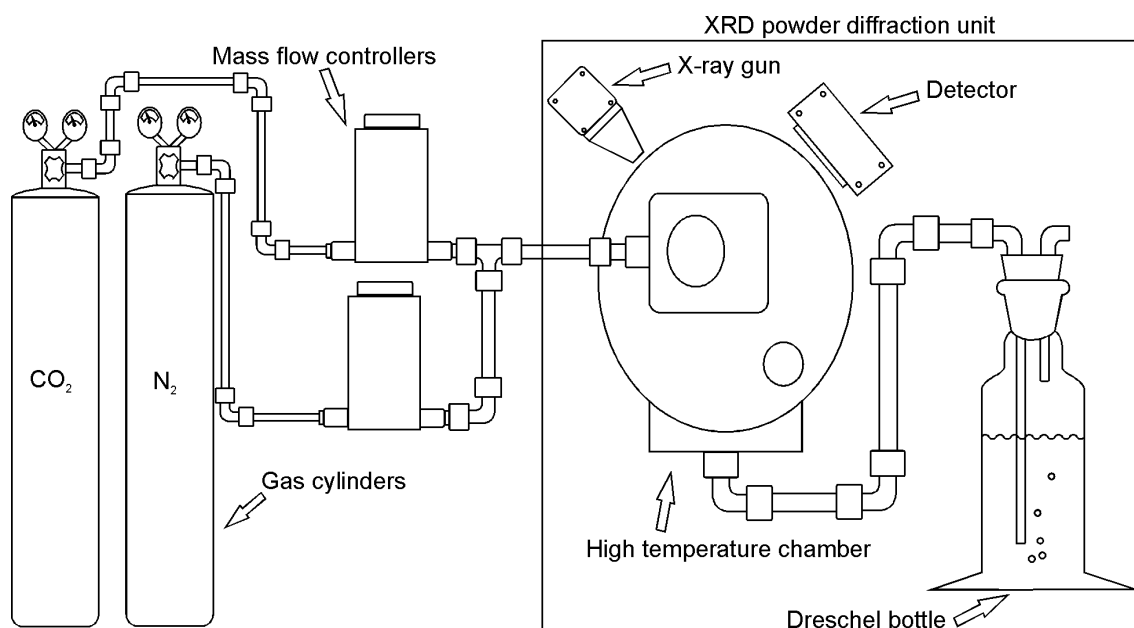


Figure 15. Schematic of the *in situ* XRD experimental setup at Leeds. The equipment on the left hand side was placed outside the XRD powder diffraction unit while the equipment enclosed within the rectangle on the right hand side was placed inside the XRD powder diffraction unit.

Diffractograms were collected from the 2θ range 14.993 - 130.000° using $\text{CuK}\alpha$ radiation with a continuous scan at a scan speed of $0.190986^\circ \text{ s}^{-1}$ for a total of 10 min and 16s. 12 such scans were carried out back to back for a total scan time of 2h, 3 min and 12s. The temperature was increased, and diffraction patterns were collected at 25, 200, 300, 400, 500, 600, 700, and 800°C respectively. A heating rate of $40^\circ\text{C min}^{-1}$ was employed between each temperature. In order to accurately gauge the effect of peak broadening, a Si standard (NIST, SRM 640b) was measured at room temperature, within the sample environment. A refinement of this data was used to determine the effects of instrumental broadening, using ICDD (International Centre for Diffraction Data) 04-007-8736.

Rietveld refinement was carried using the collected diffractograms using X'Pert Highscore Plus software (Panalytical, The Netherlands). Details of this method can be found elsewhere.^{74, 75}

High resolution synchrotron diffraction data at the Diamond Light Source (Didcot, UK) was collected for the partially hydrated material using beamline I11.⁷⁶ This data was collected from powder loaded into a 0.5 mm diameter capillary, which was sealed in ambient air and measured at room temperature. A Rietveld refinement was subsequently performed using GSAS.⁷⁷ Data was collected in the range $2\theta = 3$ - 150° , binned in 0.001° steps. The

energy of the radiation used was 15 keV ($\lambda \sim 0.826 \text{ \AA}$). Within GSAS, profile function 3 was used, and with the profile options P, Y and γ_{11} , γ_{22} , γ_{33} , γ_{12} , γ_{13} and γ_{23} were refined in order to simulate the anisotropic broadening.

Transmission electron microscopy (TEM) was conducted on an FEI Tecnai F20 operating at 200 kV and equipped with a Gatan Orius SC600A CCD camera. The sample was prepared for TEM analysis by dispersion in hexane. A drop of this dispersion (taken immediately following sonication to allow for distribution of particles throughout the hexane) was placed on a copper grid coated with a holey carbon film (Agar Scientific Ltd).

5 Conclusions

In situ XRD, in conjunction with phase quantification using Rietveld analysis, was used to successfully study the CO₂ capture of CaO and Ca(OH)₂ as well as in partially hydrated CaO, in a flow of CO₂. The results were compared to data collected using TGA, and found to be in good agreement. We observed that both the pure CaO and partially hydrated materials transformed to ca. 65% by weight, and that the pure Ca(OH)₂ converted to 100 wt% calcite at a temperature of 600 °C.

The strength of XRD is that the concentration of multiple phases can be monitored during CO₂ capture in materials such as the partially hydrated CaO reported here. In order to verify the results, calibration of five carefully prepared materials with different Ca(OH)₂/CaCO₃ ratios was performed; the resultant refinements were in excellent agreement with recorded weightings.

There are a number of additional key findings:

1. Ca(OH)₂ converted directly to 100% CaCO₃ without the formation of a CaO intermediate, as determined within the timescale of the XRD measurements.
2. Partially hydrated CaO (33.6 wt% Ca(OH)₂) reached the same CaCO₃ conversion as pure CaO. It was observed that in the mixture, the hydroxide transformed far more readily to the carbonate such that at ca. 600 °C, only CaO and CaCO₃ remained. At 800 °C, both mixtures, which comprised just CaO and CaCO₃, achieved the same capture threshold.
3. Amorphous materials were not observed for any of the materials studied. This suggests that the changes from oxide to carbonate and from hydroxide to carbonate were highly correlated and that all phases were entirely crystalline.

4. High resolution synchrotron diffraction was been used to precisely quantify the anisotropic broadening observed in the $\text{Ca}(\text{OH})_2$ phase using XRD. The determined crystallite size of 75×16 nm was in excellent agreement with observations with the TEM (average size of 75 crystallites, 83×16 nm).
5. In order to minimise the lattice strain, $\text{Ca}(\text{OH})_2$ forms an (001) orientated shell onto a CaO core, and grows preferentially in the (100) direction. The strain in the $\text{Ca}(\text{OH})_2$ crystal lattice in the partially hydrated material was 20 times larger than its yield strength in the (100) direction, leading to fracture and the generation of nano-sized crystallites.

6 Acknowledgments

RCUK councils and the Energy programme are gratefully acknowledged for grant EP/G01244X/1. This work was carried out with the support of the Diamond Light Source. Thanks to Dr Amanda Lea-Langton for samples preparation to the Beamline I11 experiment. Thanks as well to Professor Chiu Tang at Diamond Light Source and Dr Eric Lewis at the School of Physics and Astronomy for helpful discussions.

7 References

- 1 J.C. Abanades, M. Alonso and N. Rodríguez, *Ind. Eng. Chem. Res.*, 2011, **50**, 6972-6981.
- 2 J.C. Abanades, M. Alonso, and N. Rodriguez, *Int. J. Greenh. Gas Con.*, 2011, **5**, 512-520.
- 3 M. Alonso, N. Rodríguez, B. González, B. Arias and J.C. Abanades, *Ind. Eng. Chem. Res.*, 2011, **50**, 6982-6989.
- 4 B. Balasubramanian, A. Lopez Otriz, S. Kaytakoglu and D.P. Harrison, *Chem. Eng. Sci.*, 1999, **54**, 3543-3552.
- 5 N.H. Florin and A.T. Harris, *Chem. Eng. Sci.*, 2008, **63**, 287-316.
- 6 I. Martínez, R. Murillo, G. Grasa, N. Rodríguez and J.C. Abanades, *Int. J. Greenh. Gas Con.*, 2011, **5**, 498-504.
- 7 M. Widyawati, T.L. Church, N.H. Florin and A.T. Harris, *Int. J. Hydrogen Energy.*, 2011, **36**, 4800-4813.

- 8 J. Xu, J. Jianchun, C. Jie and S. Yunjuan, *Bioresource Technol.*, 2010, **101**, 5586-5591.
- 9 B. Yoosuk, P. Udomsap and B. Puttasawat, *Appl. Catal., A.*, 2011, **395**, 87-94.
- 10 R. Zhang, W. Jiang, L. Cheng, B. Sun, D. Sun and J. Bi, *Int. J. Hydrogen Energy.*, 2010, **35**, 11810-11815.
- 11 A.L. Da Silva and I.L. Müller, *Int. J. Hydrogen Energy.*, 2011, **36**, 2057-2075.
- 12 J. Li, H. Yu, G. Yang, F. Peng, D. Xie, H. Wang and J. Yang, *J. Energ. Fuel.*, 2011, **25**, 2643-2650.
- 13 B. Dou, G. Rickett, V. Dupont, P.T. Williams, H. Chen, Y. Ding and M. Ghadiri, *Bioresource Technol.*, 2010, **101**, 2436-2442.
- 14 X. Wang, M. Li, S. Li, H. Wang, S. Wang and X. Ma, *Fuel Process. Technol.*, 2010, **91**, 1812-1818.
- 15 P. Agrinier, A. Deutsch, U. Schärer and I. Martinez, *Geochim. Cosmochim. Ac.*, 2001, **65**, 2433-2632.
- 16 US Geological Survey. *Mineral Commodity Summary 2011*. Available online at www.usgs.gov.
- 17 Q. Wang, J. Luo, Z. Zhong and A. Borgna, *Energy Environ. Sci.*, 2011, **4**, 42-55.
- 18 J.C. Abanades, *Chem. Eng. J.*, 2002, **90**, 303-306.
- 19 P.S. Fennell, R. Pacciani, J.S. Dennis, J.F. Davidsson and A.N. Haryhurst, *Energ. Fuel.*, 2007, **21**, 2072-2081.
- 20 A.I. Lysikov, A.N. Salanov and A.G. Okunev, *Ind. Eng. Chem. Res.*, 2007, **46**, 4633-4638.
- 21 J.S. Wang and E.J. Anthony, *Ind. Eng. Chem. Res.*, 2005, **44**, 627-629.
- 22 A. MacKenzie, D.L. Granatstein, E.J. Anthony and J.C. Abanades, *Energ. Fuel.*, 2007, **21**, 920-926.
- 23 C. Liu, S. Shih and T. Huang, *Ind. Eng. Chem. Res.*, 2010, **49**, 9052-9057.
- 24 F. Donat, N.H. Florin, E.J. Anthony and P.S. Fennell, *Environ. Sci. Technol.*, 2012, **46**, 1262-1269.

- 25 P.S. Fennell, J.F. Davidson, J.S. Dennis and A.N. Hayhurst, *J. Energy Inst.*, 2007, **80**, 116-119.
- 26 J. Blamey, N.P.M. Paterson, D.R. Dugwell, P. Stevenson and P.S. Fennell, *P. Combust. Inst.*, 2011, **33**, 2673-2681.
- 27 V. Manovic and E.J. Anthony, *Environ. Sci. Tech.*, 2007, **41**, 1420-1425.
- 28 V. Manovic and E.J. Anthony, *Fuel.*, 2011, **90**, 233-239.
- 29 J. Blamey, N.P.M. Paterson, D.R. Dugwell and P.S. Fennell, *Energ. Fuel.*, 2010, **24**, 4605-4616.
- 30 I. Martínez, G. Grasa, R. Murillo, B. Arias and J.C. Abanades, *Energ. Fuel.*, 2011, **25**, 1294-1301.
- 31 V. Materić, S. Edwards, S.I. Smedley and R. Holt, *Ind. Eng. Chem. Res.*, 2010, **49**, 12429-12434.
- 32 J. Blamey, D.Y. Lu, P.S. Fennell and E.J. Anthony, *Ind. Eng. Chem. Res.*, 2011, **50**, 10329-10334.
- 33 J.S. Dennis and A.N. Hayhurst, *Chem. Eng. Sci.*, 1987, **42**, 2361-2372.
- 34 Z. Li, N. Cai, Y. Huang and H. Han, *Energ. Fuel.*, 2005, **19**, 1447-1452.
- 35 Z. Li, N. Cai and Y. Huang, *Ind. Eng. Chem. Res.*, 2006, **45**, 1911-1917.
- 36 N. Hildenbrand, J. Readman, I.M. Dahl and R. Blom, *Appl. Catal. A-Gen.*, 2006, **303**, 131-137.
- 37 G. Montes-Hernandez, A. Pommerol, F. Renard, P. Beck, E. Quirico and O. Brissaud, *Chem. Eng. J.*, 2010, **161**, 250-256.
- 38 R. Koirala, K.R. Gunugunuri, S.E. Pratsinis and P.G. Smirniotis, *J. Phys. Chem. C.*, 2011, **115**, 24804-24812.
- 39 S. Xu, B. Zhang, Z. Chen, J. Yu, D.G. Evans and F. Zhang, *Ind. Eng. Chem. Res.*, 2011, **50**, 6567-6572.

- 40 B.D. Cullity and S.R. Stock, *Elements of X-Ray Diffraction, third ed.*, Prentice Hall, New Jersey, 2001.
- 41 C. Rodriguez-Navarro, K. Kudlacz and E. Ruiz-Agudo, *Am. Mineral.*, 2012, **97**, 38-51.
- 42 K. Efimov, O. Czuprat and A. Feldhoff, *Solid State Chem.*, 2011, **184**, 1085-1089.
- 43 A. Lucas, M. Mouallem-Bahout, C. Carel, J. Gaudé and M. Matecki, *J. Solid State Chem.*, 1999, **146**, 73-78.
- 44 W. Liu, J.S. Dennis, D.S. Sultan, S.A.T. Redfern and S.A. Scott, *Chem. Eng. Sci.*, 2012, **69**, 644-658.
- 45 P. Engler, M.W. Santana, M.L. Mittleman and D. Balazs, *Thermochim. Acta.*, 1989, **140**, 67-76.
- 46 J. García-Martínez, A. Bueno-López, A. García-García and A. Linares-Solano, *Fuel*, 2002, **81**, 305-313.
- 47 L. Vielle, I. Rousselot, F. Leroux, J.-P. Besse and C. Taviot-Guého, *Chem. Mater.*, 2003, **15**, 4361-4368.
- 48 M. Fernández-García, X. Wang, C. Belver, A. Iglesias-Juez, J.C. Hanson and J.A. Rodriguez, *Chem. Mater.*, 2005, **17**, 4181-4193.
- 49 J.A. Rodriguez, X. Wang, J.C. Hanson, G. Liu, A. Iglesias-Juez and M. Fernández-García, *J. Chem. Phys.*, 2003, **119**, 5659-5669.
- 50 R.J. Hill and C.J. Howard, *J. Appl. Crystallogr.*, 1987, **20**, 467-474.
- 51 D.L. Bish and J.E. Post, *Am. Mineral.*, 1993, **78**, 932-940.
- 52 C.G. Kontoyannis and N.V. Vagenas, *Analyst.*, 2000, **125**, 251-255.
- 53 S. Walspurger, P.D. Cobden, W.G. Haije, R. Westerwaal, G.D. Elzinga and O.V. Safonova, *Eur. J. Inorg. Chem.*, 2010, **2010**, 2461-2464.
- 54 S. Walspurger, P.D. Cobden, O.V. Safonova, Y. Wu and E.J. Anthony, *Chem. Eur. J.*, 2010, **16**, 12694-12700.
- 55 E. Jansen, W. Schäfer and G. Will, *J. Appl. Crystallogr.*, 1994, **27**, 492-496.

- 56 J.R. Hill and R.X. Fischer, *J. Appl. Crystallogr.*, 1990, **23**, 462-468.
- 57 L.B. McCusker, R.B. Von Dreele, D.E. Cox, D. Louër and P. Scardi, *J. Appl. Crystallogr.*, 1999, **32**, 36-50.
- 58 R.H. Borgwardt and K.R. Bruce, *AIChE J.*, 1986, **32**, 239-246.
- 59 P. Sun, J.R. Grace, C.J. Lim and E.J. Anthony, *AIChE J.*, 2007, **53**, 2432-2442.
- 60 O. Chaix-Pluchery, J. Bouillot, D. Ciosmak, J.C. Niepce and F. Freund, *J. Solid State Chem.*, 1983, **50**, 247-255.
- 61 S.F. Wu, T.H. Beum and J.N. Kim, *Ind. Eng. Chem. Res.*, 2007, **46**, 7896-7899.
- 62 R.W. Cheary and A.A. Coelho, *J. Appl. Crystallogr.*, 1998, **31**, 851-861.
- 63 G.K. Williamson and W.H. Hall, *Acta Metall. Mater.*, 1953, **1**, 22-31.
- 64 J.J. Beaudoin, *Cement Concrete Res.*, 1983, **13**, 319-324.
- 65 R. Barker, *J. Appl. Chem. Biotechnol.*, 1973, **23**, 733-742.
66. S. Baruah and J. Dutta, *Sci. Technol. Adv. Mater.*, 2009, **10**, 013001.
- 67 H. Xu, Y. Zhao, S.C. Vogel, L.L. Daemen and D.D. Hickmott, *J. Solid State Chem.*, 2007, **180**, 1519-1525.
- 68 T. Ungár, *Scripta Mater.*, 2004, **51**, 777-781.
- 69 I. Martinez, G. Grasa, R. Murillo, B. Arias and J.C. Abanades, *Energ. Fuel.*, 2012, **26**, 1432-1440.
70. N.Y. Hu and A.W. Scaroni, *Fuel*, 1996, **75**, 177-186.
- 71 R. Barker, *J. Appl. Chem. Biotechnol.*, 1974, **24**, 221-227.
- 72 G.S. Grasa and J.C. Abanades, *Ind. Eng. Chem. Res.*, 2006, **45**, 8846-8851.
- 73 S. Lin, Y. Wang and Y Suzuki, *Energ. Fuel.*, 2009, **23**, 2855-2861.
- 74 N. Meethong, H.Y.S. Huang, S.A. Speakman, W.C. Carter and Y.M. Chiang, *Adv. Funct. Mater.*, 2007, **17**, 1115-1123.

75 Z. Wang, T.P. Comyn, M. Ghadiri and G.M. Kale, *J. Mater. Chem.*, 2011, **21**, 16494-16499.

76 S.P. Thompson, J.E. Parker, J. Potter, T.P. Hill, A. Birt, T.M. Cobb, F. Yuan and C.C. Tang, *Rev. Sci. Instrum.*, 2009, **80**, 075107.

77 A.C. Larson, and R.B. Von Dreele, *General Structure Analysis System, GSAS*, Los Alamos National Laboratory Report LAUR 86-748, Los Alamos, 2004.